

Nonlinear viscous higher harmonics generation due to incident and reflecting internal wave beam collision

Anil A. Aksu

Citation: [Physics of Fluids](#) **29**, 096603 (2017); doi: 10.1063/1.5001969

View online: <http://dx.doi.org/10.1063/1.5001969>

View Table of Contents: <http://aip.scitation.org/toc/phf/29/9>

Published by the [American Institute of Physics](#)

**COMPLETELY
REDESIGNED!**



**PHYSICS
TODAY**

Physics Today Buyer's Guide
Search with a purpose.

Nonlinear viscous higher harmonics generation due to incident and reflecting internal wave beam collision

Anil A. Aksu^{a)}

TUBITAK Space Technologies Research Institute, Cankaya, Ankara 06800, Turkey and Engineering Science Department, Middle East Technical University, Cankaya, Ankara 06800, Turkey

(Received 18 April 2017; accepted 26 August 2017; published online 19 September 2017)

In this paper, we have considered the non-linear effects arising due to the collision of incident and reflected internal wave beams. It has already been shown analytically [Tabaei *et al.*, “Nonlinear effects in reflecting and colliding internal wave beams,” *J. Fluid Mech.* **526**, 217–243 (2005)] and numerically [Roddenborn *et al.*, “Harmonic generation by reflecting internal waves,” *Phys. Fluids* **23**, 026601 (2011)] that the internal wave beam collision generates the higher harmonics and mean flow in a linear stratification. In this paper, similar to previous analytical work, small amplitude wave theory is employed; however, it is formulated from energetics perspective which allows considering internal wave beams as the product of slowly varying amplitude and fast complex exponential. As a result, the mean energy propagation equation for the second harmonic wave is obtained. Finally, a similar dependence on the angle of incidence is obtained for the non-linear energy transfer to the second harmonic with previous analyses. A possible physical mechanism for this angle dependence on the second harmonic generation is also discussed here. In addition to previous studies, the viscous effects are also included in the mean energy propagation equation for the incident, the reflecting, and the second harmonic waves. Moreover, even though the mean flow obtained here is only confined to the interaction region, it is also affected by viscosity via the decay in the incident and the reflecting internal wave beams. Furthermore, a framework for the non-linear harmonic generation in non-linear stratification is also proposed here. *Published by AIP Publishing.* [<http://dx.doi.org/10.1063/1.5001969>]

I. INTRODUCTION

When the fluid density is continuously stratified, the oscillatory motion can occur due to differences in buoyancy¹² with a frequency ω . These types of waves are commonly called internal gravity waves. In contrast to surface waves, internal waves are not restricted to the interface; they can also propagate vertically.^{12,15} In the absence of background flow, the dispersion relation of linear internal plane waves can be given as

$$\omega^2 = \frac{N^2 k_x^2}{k_x^2 + k_z^2}, \quad (1)$$

where k_x , k_z are the wave numbers in the x and z directions and $N = \sqrt{(-g/\rho_0)(d\bar{\rho}/dz)}$ is the buoyancy frequency, where $d\bar{\rho}/dz$ is the vertical density gradient and ρ_0 is the characteristic density of the stratified fluid. This relation determines both the angle of propagation of an internal wave beam and the direction of the wave number vector. Furthermore, there are several ways that internal gravity waves are generated. The internal waves can be generated by flow over topography. Initially, barotropic tidal currents result in baroclinic motion when it interacts with the topography. During the conversion of the energy from barotropic to the baroclinic currents, internal wave beams radiate from the topography. In general, the internal waves produced do not have a particular forcing frequency but a spectrum of frequencies.¹⁸ 10% of the total energy of

the currents is transferred to the internal waves.⁷ This energy transfer could have a considerable impact on the mixing of total energy in the deep ocean.^{7,18}

The interaction with the topography creates high modes which have high wave numbers and low modes which have low wave numbers. Only the low modes travel far from the region they are generated.⁷ The topographic generation mechanism should be introduced into the numerical model used to study the evolution of an internal wave beam. Recently, considerable attention is paid to understand generation mechanisms of internal waves numerically^{5,14,23} and experimentally.² In numerical simulations, a virtual forcing region is used to approximate the topographic mechanism.^{5,14,23} In the experimental setup, a mechanical forcing pedal located on a boundary is used in the recent study by Allshouse *et al.*²

The generation mechanism is one aspect of the subject. However, the fate of a generated internal wave beam is determined by the several other factors like non-linearity, viscous dissipation, and the buoyancy frequency profile in the vertical direction. The effect of non-linearity is felt via several ways. The non-linear effects of internal wave propagation are paid specific attention recently. The non-linear effects are commonly observed in the case of the non-linear stratification which is also a more accurate representative of real oceanic conditions which commonly includes a linearly stratified lower layer, a pycnocline region where the buoyancy frequency reaches its maximum and a well-mixed upper layer where the buoyancy frequency is negligible.¹³ One of the interesting observations of the

^{a)}Electronic mail: anil.aksu@tubitak.gov.tr

non-linear effects is the formation of the solitary waves, for example, in the Bay of Biscay.³ Solitary internal waves are also obtained numerically.^{6,9,11} The existence of solitary waves is one aspect of nonlinearity; in such waves, nonlinearity balances the effect of dispersion.¹⁰ Moreover, the non-linearity may also generate higher harmonics^{1,5,14,17,20–22} and mean flow.^{4,17,23}

It is already shown that the internal wave beam collision in a linear stratification generates higher harmonics.^{1,17} Internal waves with the same frequency, interacting non-linearly in a linear stratification where buoyancy frequency is constant, generate the second harmonic wave^{14,17} and the mean flow.^{17,23} The same non-linear interaction between two internal waves with frequencies ω_1 and ω_2 in a linear stratification generates internal waves with frequencies $\omega_1 + \omega_2$ and $\omega_1 - \omega_2$.¹⁷ However, if the frequency of the non-linearly generated internal wave beam is higher than the buoyancy frequency, that wave beam is evanescent.

As stated earlier, the non-linear stratification is a more realistic model of an ocean. This type of stratification may also have linear effects which may be indirectly effective on higher harmonics and mean flow generation in the case of an internal wave beam collision. The non-uniformity in stratification not just leads to refraction but also to internal wave beam energy accumulation or diminution along the ray path.¹³ Also, the forcing of the second harmonic wave and mean flow is in the order of the square of the incident internal wave beam amplitude.¹⁷ As a result, the energy accumulation or diminution may affect how much energy is transferred to higher harmonics and mean flow. Furthermore, it is shown that the amplitude of an internal wave beam attenuates along the ray path due to weak viscous decay.¹² This viscous dissipation is caused by spatio-temporal oscillations along the ray path. These spatio-temporal oscillations are highly dependent on the buoyancy frequency which reaches its peak around the pycnocline. The increase in the buoyancy frequency leads to larger wave number in the vertical direction which can be obtained via the dispersion relation given in Eq. (1). As a result, in the case of pycnocline, since the wave number vector affects the viscous dissipation exponentially,¹² the viscous effects may be non-negligible. Therefore, the inviscid analysis may not give a correct representative of the real situation in the ocean.

In the previous studies on the non-linear higher harmonics and mean flow generation,^{5,17} the effects of the viscous dissipation and the energy accumulation or diminution due to the non-uniform stratification are not discussed. These effects may become important in the case of internal wave propagation and generation in non-uniform stratification. The main motivation behind the present work is to derive a theoretical model for higher harmonics generation which can include the effects of viscous dissipation and the energy accumulation or diminution along the ray path. Furthermore, this type of problem requires an approach that solves the whole field to include the effects mentioned above whereas the existing inviscid model¹⁷ gives the far field response via radiation conditions.

In the analysis presented here, differing from previous theoretical models,^{5,16,17} the time averaged energy flux formulation is used. In this formulation, the group velocities

explicitly appear. Therefore, the need of imposing radiation conditions is avoided. The main assumption in the theoretical model used here is that the velocity field, the perturbation pressure field, and the perturbation density field can be represented as the product of amplitude multiplied with a complex exponential.¹⁹ The complex exponential part is a function of phase variables which are wave number vector and frequency. These phase variables are assumed to be fast variables. At the same time, the amplitudes of these fields are governed by slow variables which translate with group velocities.¹⁹ The main idea behind the slow variable and fast variable representation is that the spatial gradients of the amplitude envelope are much smaller than the spatial gradients of the phase variables. Therefore, slow and fast variables can be treated separately. Also, the weak viscous effects are neglected in phase variables which have a relatively small effect on the dispersion relation as shown by Ghaemsaidi.⁸ However, the effect of viscosity is considered in the mean energy flux equations. Finally, to understand the dependence on the angle incidence of the incident internal wave beam of the second harmonic generation found previously by Tabaei, Akyolas, and Lamb¹⁷ (hereafter referred to as TAL), the energy transfer rate from the incident internal wave beam to the second harmonic wave beam is analyzed for the various angles of incidence. Therefore, even though it is not solved for non-uniform stratification, a framework which can be extended to non-uniform stratification such as a finite pycnocline case is developed.

This manuscript is organized as follows. The propagation and the attenuation of the incident internal wave beam are analyzed in Sec. II. In Sec. III, the reflection of the internal wave beam from the free slip surface is discussed. Section IV introduces an alternative formulation of the second harmonic generation mechanism due to the incident and the reflecting internal wave beam collision. In addition to the previous theoretical approach,¹⁷ this formulation also includes weak viscous effects and does not need imposing radiation conditions. The governing differential equation for the second harmonic wave is solved both analytically and numerically for various angles of incidence. The mean flow generation in the interaction region is analyzed in Sec. V. The results are presented in Sec. VI. The normalized second harmonic energy fluxes are compared with the inviscid model.¹⁷ A close correlation between them is observed. Since the analysis in the present study does not need radiation conditions, not only the far field response but also the entire field is obtained for the second harmonic wave beam. Additionally, the subsurface mean flow profile generated by the internal wave beam collision is similar to the previous inviscid results. Finally, Sec. VII discusses the dependence on the angle of incidence of the second harmonic generation and the physical mechanism behind it.

II. VISCOUS INTERNAL WAVE BEAM PROPAGATION BEFORE INTERNAL WAVE BEAM COLLISION

The internal wave beams generated by the interaction between a tidal current with topography as explained by Garrett and Kunze⁷ can be in various forms. In some numerical simulations, this generation mechanism can be replaced with a

virtual forcing pedal as shown by Diamessis *et al.*,⁵ and Zhou and Diamessis²³ to generate an internal wave beam with a specified wave number and frequency. Therefore, the governing equations with a virtual forcing pedal can be given as

$$\frac{\partial u}{\partial x} + \frac{\partial w}{\partial z} = 0, \quad (2)$$

$$\frac{\partial \mathbf{u}}{\partial t} + N(\mathbf{u}) = -\frac{1}{\rho_0} \nabla p + \nu \nabla^2 \mathbf{u} + \mathbf{F}_g, \quad (3)$$

$$\frac{\partial \rho}{\partial t} + N_\rho(\rho, \mathbf{u}) = w \frac{\rho_0}{g} N^2 + \mathbf{F}_\rho, \quad (4)$$

where $\mathbf{u} = (u, w)$ is the velocity field, p and ρ are the perturbation pressure and density, $\mathbf{F}_g = -\rho g \vec{k}/\rho_0$, and \mathbf{F}_u and \mathbf{F}_ρ are the virtual forcing pedal terms given in detail in Appendix A, $N(\mathbf{u})$ and $N_\rho(\rho, \mathbf{u})$ are the non-linear terms provided in detail in Appendix B. The velocity, the perturbation pressure, and the perturbation density fields can be decomposed into four parts as

$$\mathbf{u} = \epsilon(\mathbf{u}_{inc}^{\omega_0} + \mathbf{u}_{ref}^{\omega_0}) + \epsilon^2(\mathbf{u}^{2\omega_0} + \mathbf{u}^0), \quad (5)$$

$$p = \epsilon(p_{inc}^{\omega_0} + p_{ref}^{\omega_0}) + \epsilon^2(p^{2\omega_0} + p^0), \quad (6)$$

$$\rho = \epsilon(\rho_{inc}^{\omega_0} + \rho_{ref}^{\omega_0}) + \epsilon^2(\rho^{2\omega_0} + \rho^0), \quad (7)$$

where ϵ is the small perturbation parameter and *inc* subscript stands for the incident primary frequency wave beam, *ref* subscript stands for the reflecting primary frequency wave beam, $2\omega_0$ superscript stands for the second harmonic wave beam, and 0 superscript stands for the mean flow. The field variables given above can be given as the multiplication of the fast complex exponential part and amplitude part where amplitude varies slowly.¹⁹ Here ϵ serves as a small parameter where $\epsilon = (\sigma k_\eta)^{-1} \ll 1$. It should also be noted that $k_\eta = \sqrt{k_x^2 + k_z^2}$ and σ is the half width of the wave amplitude. This virtual forcing pedal generates incident internal wave beams in the following form:

$$\begin{aligned} \mathbf{u}_{inc}^{\omega_0} &= Re(\vec{A}_{inc}(X_{inc}, Z_{inc}, T)e^{i\phi_{inc}}) \\ &= \vec{A}_{inc}(X_{inc}, Z_{inc}, T) \cos \phi_{inc}, \end{aligned} \quad (8)$$

$$\begin{aligned} p_{inc}^{\omega_0} &= Re(P_{inc}(X_{inc}, Z_{inc}, T)e^{i\phi_{inc}}) \\ &= P_{inc}(X_{inc}, Z_{inc}, T) \cos \phi_{inc}, \end{aligned} \quad (9)$$

$$\begin{aligned} \rho_{inc}^{\omega_0} &= Re(\varrho_{inc}(X_{inc}, Z_{inc}, T)e^{i(\phi_{inc}-\pi/2)}) \\ &= \varrho_{inc}(X_{inc}, Z_{inc}, T) \sin \phi_{inc}, \end{aligned} \quad (10)$$

where the fast variable $\phi_{inc} = k_x x - k_z z - \omega t$ and the slow variables $X_{inc} = \epsilon(x - C_g x t)$, $Z_{inc} = \epsilon(z - C_g z t)$, $T = \epsilon^2 t$, and $\vec{C}g = \partial \omega / \partial k_x \vec{i}, \partial \omega / \partial k_z \vec{k}$. It should also be noted that according to the linear theory,¹⁵ the perturbation pressure field and the velocity field are in phase; however, the perturbation density field and the velocity field are out of phase. Therefore, there is a phase angle $\pi/2$ between them. Each velocity field has to satisfy the continuity equation separately. The primary frequency velocity field is composed of the incident and the reflecting velocity fields which propagate along different ray paths; therefore, except for the interaction region, they are effective in different parts of the domain. Since the continuity condition has to be satisfied in the entire domain, the incident

and the reflecting velocity fields have to satisfy the continuity condition separately. After applying the continuity condition (2) to the velocity profile for the incident internal wave beam, the relation between the velocity amplitudes can be obtained as

$$A_{inc}^x k_x = A_{inc}^z k_z. \quad (11)$$

In total, using the velocity field and the perturbation density field, the time-averaged kinetic energy $\langle E_k \rangle$ and the time-averaged potential energy $\langle E_p \rangle$ can be obtained. By using the definition of the total energy,² the time averaged total energy can be obtained as

$$\begin{aligned} \langle E_k \rangle + \langle E_p \rangle &= \frac{1}{2} \left(\epsilon^2 \frac{\rho_0}{2} \frac{\omega}{2\pi} \int_0^{2\pi/\omega} \mathbf{u}_{inc}^{*\omega_0} \mathbf{u}_{inc}^{\omega_0} dt \right. \\ &\quad \left. + \epsilon^2 \frac{g^2}{2\rho_0 N_0^2} \frac{\omega}{2\pi} \int_0^{2\pi/\omega} \rho_{inc}^{*\omega_0} \rho_{inc}^{\omega_0} dt \right). \end{aligned} \quad (12)$$

In the absence of the Coriolis force, in a linear internal wave field, the kinetic energy and available potential energy are equally partitioned.¹⁵ Therefore, the total energy defined in Eq. (12) can be given as

$$\langle E \rangle = \langle E_k \rangle + \langle E_p \rangle = \epsilon^2 \frac{\rho_0}{2} (\vec{A}_{inc} \cdot \vec{A}_{inc}). \quad (13)$$

The mean total energy flux is also defined as the product of the pressure field with the velocity¹⁵ as follows:

$$\epsilon^2 \langle p_{inc}^{\omega_0} \mathbf{u}_{inc}^{\omega_0} \rangle = \langle E \rangle \vec{C}g. \quad (14)$$

The contribution of the kinetic energy can be obtained by taking the time averaged product of Eq. (3) and the complex conjugate of the velocity field as follows:

$$\langle \mathbf{u}_{inc}^{*\omega_0} \left(\frac{\partial \mathbf{u}_{inc}^{\omega_0}}{\partial t} \right) \rangle = -\frac{1}{\rho_0} \nabla p + \nu \nabla^2 \mathbf{u}_{inc}^{\omega_0} + \mathbf{F}_g + \mathbf{F}_u \rangle. \quad (15)$$

It should be noted that non-linear terms are neglected in Eq. (15) as the generation region of the incident internal wave beam is far from the interaction region. Therefore, the non-linear effects are negligible in the generation of the incident internal wave beam. Moreover, here the main properties that allow to formulate the mean energy flow equations are time scales and phase relations. The evolution of the internal wave beam amplitude is slow in time and space; however, the complex exponential part is fast in time and space. Therefore, the averaging over one wave period $\omega/2\pi$ would enable to reduce to the time scale of the analysis to the slow time. In addition, \mathbf{F}_g and the velocity field are out of phase; therefore, the time averaging cancels out. After performing the time averaging operations, the mean kinetic energy flow equation is obtained as

$$\frac{\partial \langle E_k \rangle}{\partial t} + \nabla \cdot (\vec{C}g \langle E \rangle) = -\frac{\nu N^2 k_x^2}{\omega^2} \langle E \rangle + \frac{2\epsilon \rho_0 U_f k_z}{T k_x} A_{inc}^x F. \quad (16)$$

Similarly, the contribution to the available potential energy by virtual forcing can be obtained by multiplying the energy equation (4) by the conjugate of the perturbation density $\rho_{inc}^{*\omega_0}$; however it should also be multiplied with the factor $g^2/2\rho_0 N_0^2$. It results in the following operation:

$$\frac{g^2}{2\rho_0 N_0^2} \langle \rho_{inc}^{*\omega_0} \left(\frac{\partial \rho_{inc}^{\omega_0}}{\partial t} \right) \rangle = w_{inc} \frac{\rho_0}{g} N_0^2 + \mathbf{F}_\rho \rangle. \quad (17)$$

After performing the operation described in Eq. (17), the time-averaged available potential energy is obtained as

$$\frac{\partial \langle E_p \rangle}{\partial t} = \frac{\epsilon g U_f}{2\omega T} \varrho_{inc} F = \frac{\epsilon \rho_0 N_0^2 U_f k_x}{2\omega^2 T k_z} A_{inc}^x F. \quad (18)$$

Since the analysis above is performed in the region where the non-linear effects are negligible, the envelope of the perturbation density field ϱ_{inc} and the envelope of the velocity field in the x direction A_{inc}^x can be related as

$$\varrho_{inc} = \frac{\rho_0 N_0^2 k_x}{g \omega k_z} A_{inc}^x. \quad (19)$$

However, the energy equations for the potential and kinetic energy can not be evaluated separately. The virtual forcing region for the potential energy and the kinetic energy contributes to total energy, and the energy is equally distributed between the kinetic and the available potential energy in the absence of the rotating frame. As a result, the total energy equation is obtained by adding Eqs. (16) and (18) and it results in the following total energy equation:

$$\begin{aligned} \frac{\partial \langle E \rangle}{\partial t} + \nabla \cdot (\vec{C}g \langle E \rangle) &= -\frac{\nu N^2 k_x^2}{\omega^2} \langle E \rangle \\ &+ \left(\frac{2\epsilon \rho_0 U_f k_z}{T k_x} + \frac{\epsilon \rho_0 N_0^2 U_f k_x}{2\omega^2 T k_z} \right) A_{inc}^x F \\ &= -\frac{\nu N^2 k_x^2}{\omega^2} \langle E \rangle + \gamma A_{inc}^x F. \end{aligned} \quad (20)$$

Equation (10) governs the evolution of the energy of the incident internal wave beam; it includes the effects of viscous dissipation along the internal wave beam path. Even though it can be applied to both linear and non-linear stratifications. The effect of non-linear stratification will be felt via the group velocity $\vec{C}g$ and the viscous dissipation term $\nu N^2 k_x^2 / \omega^2$. As for the solution of Eq. (20), it can be used to obtain both transient and steady-state solutions; however, in the present study, the attention is paid on the steady-state solution. Therefore, the steady-state response of Eq. (20) can be given as

$$\nabla \cdot (\vec{C}g \langle E \rangle) = -\frac{\nu N^2 k_x^2}{\omega^2} \langle E \rangle + \gamma A_{inc}^x F. \quad (21)$$

In case of a linear stratification, the group velocity is constant along the intern wave beam path; this will enable us to simplify Eq. (21). The new coordinate system $\xi - \eta$ is introduced. η is in the direction of the wave number vector \vec{k} and ξ is in the direction of the group velocity vector $\vec{C}g$. Explicitly, the relation between the $x-z$ coordinate system and $\xi-\eta$ coordinate system can be given as

$$\begin{bmatrix} \xi \\ \eta \end{bmatrix} = \begin{bmatrix} \cos \theta & \sin \theta \\ -\sin \theta & \cos \theta \end{bmatrix} \begin{bmatrix} x \\ z \end{bmatrix}, \quad (22)$$

where $\theta = \tan^{-1}(k_x/k_z)$. According to linear theory,¹⁵ the wave number vector \vec{k} and the group velocity vector $\vec{C}g$ are orthogonal to each other; therefore, the orthogonality is recovered in the new coordinate system $\xi - \eta$. In this coordinate system, Eq. (21) can be given as

$$Cg_\xi \frac{\partial \langle E \rangle}{\partial \xi} = -\frac{\nu N^2 k_x^2}{\omega^2} \langle E \rangle + \gamma A_{inc}^x F, \quad (23)$$

where $Cg_\xi = \sqrt{Cg_x^2 + Cg_z^2}$. Moreover, the energy $\langle E \rangle$ can be written in terms of A_{inc}^x by using Eq. (13) as

$$\langle E \rangle = \epsilon^2 \frac{\rho_0}{2} \left(1 + \frac{k_x^2}{k_z^2} \right) (A_{inc}^x)^2 = \epsilon^2 \frac{\rho_0}{2} \frac{N_0^2}{\omega^2} \frac{k_x^2}{k_z^2} (A_{inc}^x)^2. \quad (24)$$

After replacing Eq. (24) into Eq. (23), the simplified equation is obtained as

$$\frac{\partial A_{inc}^x}{\partial \xi} = -\frac{\nu N_0^2 k_x^2}{2Cg_\xi \omega^2} A_{inc}^x + \frac{\gamma \omega^2 k_z^2}{\epsilon^2 Cg_\xi \rho_0 N_0^2 k_x^2} F. \quad (25)$$

In generic form, the analytical solution to Eq. (25) is given as

$$A_{inc}^x = \frac{\gamma \omega^2 k_z^2}{\epsilon^2 Cg_\xi \rho_0 N_0^2 k_x^2} \exp(-\alpha \xi) \int_{-\infty}^{\xi} \exp(\alpha \xi') F d\xi'. \quad (26)$$

Note that $\alpha = \nu N_0^2 k_x^2 / 2Cg_\xi \omega^2$. The Gaussian forcing function F described in Appendix A can also be written in the $\xi - \eta$ coordinate system as

$$F(\xi, \eta) = \exp\left(-\frac{\xi^2}{2\sigma^2} - \frac{\eta^2}{2\sigma^2}\right). \quad (27)$$

Under this type of forcing, the integral in Eq. (26) can be computed as

$$\begin{aligned} \int_{-\infty}^{\xi} \exp(\alpha \xi') F d\xi' &= \int_{-\infty}^{\xi} \exp(\alpha \xi') \exp\left(-\frac{\xi'^2}{2\sigma^2} - \frac{\eta^2}{2\sigma^2}\right) d\xi' \\ &= \frac{\sigma}{\sqrt{2\pi}} \exp\left(-\frac{\eta^2}{2\sigma^2}\right) \exp\left(\frac{(\alpha\sigma)^2}{2}\right) \\ &\times \left(\frac{1}{2} + \frac{1}{2} \operatorname{erf}\left(\frac{\xi - \alpha\sigma^2}{\sqrt{2}\sigma}\right)\right). \end{aligned} \quad (28)$$

The resultant integral gives us the distribution of the velocity amplitude along the propagation direction. Moreover this integral converges to a certain value after $\xi > 2\sqrt{2}\sigma + \alpha\sigma^2$ which can be given as

$$\begin{aligned} A_{inc}^x &= \frac{\gamma \omega^2 \sigma}{\epsilon^2 \sqrt{2\pi} Cg_\xi \rho_0 N_0^2} \exp\left(\frac{(\alpha\sigma)^2}{2}\right) \exp\left(-\frac{\eta^2}{2\sigma^2} - \alpha\xi\right) \\ &= A_0 \exp(-\alpha\xi) \exp\left(-\frac{\eta^2}{2\sigma^2}\right). \end{aligned} \quad (29)$$

After obtaining A_{inc}^x , the rest of the variables can be written in terms of the amplitude envelope of the velocity in the x direction. Therefore, the velocity field and the perturbation density field can be written as

$$u_{inc}^{\omega_0} = A_0 \exp(-\alpha\xi) \exp\left(-\frac{\eta^2}{2\sigma^2}\right) \cos \phi_{inc}(\vec{i}, \frac{k_x}{k_z} \vec{k}), \quad (30)$$

$$\rho_{inc} = \frac{\rho_0 A_0 N_0^2 k_x}{g \omega k_z} \exp(-\alpha\xi) \exp\left(-\frac{\eta^2}{2\sigma^2}\right) \sin \phi_{inc}. \quad (31)$$

Similarly, the perturbation pressure field can be obtained by using the energy flux relation given in Eq. (14) as

$$p_{inc}^{\omega_0} = \frac{\rho_0 A_0 N_0^2 Cg_\xi k_x^2}{(\omega k_z)^2} \exp(-\alpha\xi) \exp\left(-\frac{\eta^2}{2\sigma^2}\right) \cos \phi_{inc}. \quad (32)$$

III. INTERNAL WAVE BEAM REFLECTION FROM FREE SLIP SURFACE

In case of uniform stratification, the incident internal wave beam starts reflecting when it reaches the free slip surface upper boundary as depicted in Fig. 1. The incident internal wave beam deposits its energy on the reflecting part. Even though it is known that it would lead to surface waves, their effects on internal waves are negligible. The internal wave beam profile reflecting from the level $z=H$ shown in Fig. 1 can also be written in terms of fast and slow variables as

$$\mathbf{u}_{ref}^{\omega_0} = Re(\vec{A}_{ref}(X_{ref}, Z_{ref}, T)e^{i\phi_{ref}}) = \vec{A}_{ref}(X_{ref}, Z_{ref}, T) \cos \phi_{ref}, \quad (33)$$

$$\begin{aligned} p_{ref}^{\omega_0} &= Re(P_{ref}(X_{ref}, Z_{ref}, T)e^{i\phi_{ref}}) \\ &= P_{ref}(X_{ref}, Z_{ref}, T) \cos \phi_{ref}, \end{aligned} \quad (34)$$

$$\begin{aligned} \rho_{ref}^{\omega_0} &= Re(\varrho_{ref}(X_{ref}, Z_{ref}, T)e^{i(\phi_{ref}-\pi/2)}) \\ &= \varrho_{ref}(X_{ref}, Z_{ref}, T) \sin \phi_{ref}, \end{aligned} \quad (35)$$

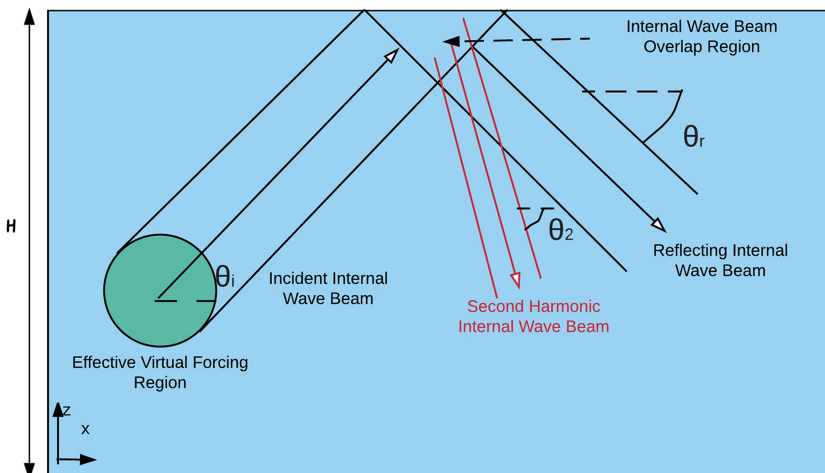
where $\phi_{ref} = k_x x + k_z z - \omega t + \phi_0$, where ϕ_0 is the phase difference, and the slow variables $X_{ref} = \epsilon(x - Cg_x t)$, $Z_{ref} = \epsilon(z + Cg_z t')$, and the slow time is independent of the direction of the propagation; therefore, the same slow time is assumed. Also, it should be noted that the perturbation pressure and the velocity field for the reflecting internal wave beam is assumed to be in-phase. However, the perturbation density field is again out of phase with the velocity field. The reflecting velocity field given in Eq. (33) also satisfies the continuity equation as

$$A_{ref}^x k_x = -A_{ref}^z k_z. \quad (36)$$

Moreover, virtual forcing is negligible in the reflection region. Therefore, the governing equation for the reflecting internal wave beam can be written as

$$\nabla \cdot (\vec{C}g_{ref} \langle E_{ref} \rangle) = -\frac{\nu N^2 k_x^2}{\omega^2} \langle E_{ref} \rangle. \quad (37)$$

The magnitude of the reflecting group velocity vector $\vec{C}g_{ref}$ is the same as the incident group velocity vector $\vec{C}g$. However, it propagates downwards; therefore, explicitly the reflecting group velocity vector can be given as $Cg_{ref}^x = Cg^x$



and $Cg_{ref}^z = -Cg^z$. Similar to the incident internal wave beam, a new coordinate system $\xi_r - \eta_r$ is introduced. Note that r subscript stands for denoting reflection. Again, η_r is in the direction of the wave number vector \vec{k} and ξ_r is in the direction of the group velocity vector $\vec{C}g_{ref}$. Explicitly, the relation between the $x-z$ coordinate system and $\xi_r - \eta_r$ coordinate system can be given as

$$\begin{bmatrix} \xi_r \\ \eta_r \end{bmatrix} = \begin{bmatrix} \cos \theta_r & \sin \theta_r \\ -\sin \theta_r & \cos \theta_r \end{bmatrix} \begin{bmatrix} x \\ z \end{bmatrix}, \quad (38)$$

where $\theta_r = \tan^{-1}(-k_x/k_z)$. Under this coordinate mapping, Eq. (37) can be written as

$$Cg_{\xi_r} \frac{\partial \langle E_{ref} \rangle}{\partial \xi_r} = -\frac{\nu N_0^2 k_x^2}{\omega^2} \langle E_{ref} \rangle. \quad (39)$$

Note that the magnitude of the group velocity of the incident internal wave beam and the reflecting internal wave beam is the same. Differing from Eq. (39), in Eq. (23), there is no external forcing term. The effect of virtual forcing is negligible in the reflection zone; because of its Gaussian property, it is only localized in a particular neighbourhood. Equation (39) can be simplified even further by expanding the total energy of the reflecting internal wave beam energy as

$$\langle E_{ref} \rangle = \epsilon^2 \rho_0 \frac{N_0^2 k_z^2}{2\omega^2 k_x^2} (A_{ref}^x)^2. \quad (40)$$

After plugging that into Eq. (39), the following simplified equation is obtained:

$$\frac{\partial A_{ref}^x}{\partial \xi_r} = -\frac{\nu N_0^2 k_x^2}{2Cg_{\xi_r} \omega^2} A_{ref}^x. \quad (41)$$

The solution to Eq. (41) can be simply given as

$$A_{ref}^x = G(\eta_r) \exp(-\alpha \xi_r). \quad (42)$$

Here, $G(\eta_r)$ is a function of only η_r variable and it is determined by the boundary condition which necessitates no mass flux at $z = H$ which can be explicitly given as

$$A_{inc}^z \cos \phi_{inc} \Big|_{z=H} + A_{ref}^z \cos \phi_{ref} \Big|_{z=H} = 0. \quad (43)$$

The relation above can also be written in terms of A_{inc}^x and A_{ref}^x as

$$A_{inc}^x \cos \phi_{inc} \Big|_{z=H} = A_{ref}^x \cos \phi_{ref} \Big|_{z=H}. \quad (44)$$

FIG. 1. Schematic of the internal wave beam with a frequency ω and a wave number vector k_x, k_z generated by a virtual forcing region. The incident internal wave beam reflects at the top of the domain where $z = H$ and the reflecting part interacts with the incident internal wave beam within the overlap region. They interact non-linearly and generate mean flow and higher harmonics with a frequency $n\omega$.

This condition requires matching of phases ϕ_{inc} and ϕ_{ref} and the amplitudes A_{inc}^x and A_{ref}^x at the level $z = H$. First, the phase matching leads to the following equality:

$$k_x x - k_z H - \omega t = k_x x + k_z H - \omega t + \phi_0. \quad (45)$$

Therefore, $\phi_0 = -2k_z H$. Moreover, the amplitude of the incident internal wave beam is already known. Therefore, the amplitude of the reflecting beam can also be obtained through the matching condition and it can be explicitly given as

$$A_{ref}^x = A_{ref} \exp(-\alpha \xi_r) \exp\left(-\frac{\eta_r^2}{2\sigma^2}\right), \quad (46)$$

where $A_{ref} = A_0 \exp(-\alpha \xi(H \tan \theta, H))$. Note that $\xi(H \tan \theta, H) = H \sin \theta + H \cos \theta$. As a result, the velocity, the perturbation pressure, and the perturbation density fields of the reflecting wave beam can be given as

$$\mathbf{u}_{ref}^{\omega_0} = A_{ref} \exp(-\alpha \xi_r) \exp\left(-\frac{\eta_r^2}{2\sigma^2}\right) \cos \phi_{ref} (\vec{i}, -\frac{k_x}{k_z} \vec{k}), \quad (47)$$

$$p_{ref}^{\omega_0} = \frac{\rho_0 A_{ref} N_0^2 C g_{\xi_r} k_x^2}{(\omega k_z)^2} \exp(-\alpha \xi_r) \exp\left(-\frac{\eta_r^2}{2\sigma^2}\right) \cos \phi_{ref}, \quad (48)$$

$$\rho_{ref} = \frac{\rho_0 A_{ref} N_0^2 k_x}{g \omega k_z} \exp(-\alpha \xi_r) \exp\left(-\frac{\eta_r^2}{2\sigma^2}\right) \sin \phi_{ref}. \quad (49)$$

So far, the non-linear effects are still not considered yet. As stated earlier, the non-linear interactions are assumed to be considerably smaller than linear interactions. The weakly non-linear analysis in the present work focuses on the incident and the reflecting internal wave beams overlap. As a result, the non-linear higher harmonics generation and the mean flow generation are expected.

IV. HIGHER HARMONIC GENERATION DUE TO INCIDENT AND REFLECTING INTERNAL WAVE BEAM COLLISION

In Secs. II and III, only linear effects are considered. These include internal wave beam propagation, reflection, and attenuation. Moreover, there are also weakly non-linear interactions. It is already shown that the non-linear interaction between the incident and the reflecting beams in the inviscid case can generate higher harmonics¹⁷ and mean flow.^{17,23} But there is a limitation to the higher harmonic generation. According to the dispersion relation (1), if the frequency of the higher harmonics $n\omega$ is higher than the buoyancy frequency N_0 , the wave number in the z direction is complex. As a result, the second harmonic wave beam is evanescent. This condition also limits the frequency of the incident internal wave beam for the generation of the second harmonic wave as follows:

$$\omega < \frac{N_0}{2}. \quad (50)$$

Therefore, this limitation means that for the angle of incidence $\theta > 30^\circ$, the higher harmonics will be evanescent. Because of this, the primary attention is paid on the cases where the angle of incidence $\theta < 30^\circ$. The propagating second harmonic is again written in terms of fast variables and slow variables as

$$\begin{aligned} \mathbf{u}^{2\omega_0} &= Re(\vec{A}_{2\omega_0}(X_{2\omega_0}, Z_{2\omega_0}, T) e^{i\phi_{2\omega_0}}) \\ &= \vec{A}_{2\omega_0}(X_{2\omega_0}, Z_{2\omega_0}, T) \cos \phi_{2\omega_0}, \end{aligned} \quad (51)$$

$$\begin{aligned} p^{2\omega_0} &= Re(P_{2\omega_0}(X_{2\omega_0}, Z_{2\omega_0}, T) e^{i\phi_{2\omega_0}}) \\ P_{2\omega_0}(X_{2\omega_0}, Z_{2\omega_0}, T) \cos \phi_{2\omega_0}, \end{aligned} \quad (52)$$

$$\begin{aligned} \rho^{2\omega_0} &= Re(\varrho_{2\omega_0}(X_{2\omega_0}, Z_{2\omega_0}, T) e^{i(\phi_{2\omega_0} - \pi/2)}) \\ &= \varrho_{2\omega_0}(X_{2\omega_0}, Z_{2\omega_0}, T) \sin \phi_{2\omega_0}, \end{aligned} \quad (53)$$

where $\phi_{2\omega_0} = 2k_x x + k_z^{2\omega_0} z - 2\omega t$ and the slow variables $X_{2\omega_0} = \epsilon(x - C g_x^{2\omega_0} t)$, $Z_{2\omega_0} = \epsilon(z + C g_z^{2\omega_0} t)$. The group velocity and the wave numbers can be computed by using a dispersion relation for the frequency 2ω and the propagation direction. Similar to the incident internal wave beam, if there are no Coriolis forces, the velocity field and the perturbation pressure field are in phase, and the perturbation density field and velocity field are out of phase in the second harmonic wave beam. Moreover, the velocity for the second harmonic signal satisfies the continuity separately. Therefore, the velocity amplitudes of the second harmonic wave in x and z can be related by the continuity equation as

$$2A_{2\omega_0}^x k_x = -A_{2\omega_0}^z k_z^{2\omega_0}. \quad (54)$$

The higher harmonics are generated in the overlap region where the incident and the reflecting internal wave beams collide. This region is far from the effective area of the virtual forcing pedal shown in Fig. 1; therefore, the effect of the virtual forcing pedal can be neglected in both momentum equations, (3) and (4), and the energy equation (5). However, in this case, the non-linear effects are not negligible. Indeed, the non-linear interaction between the incident and the reflecting internal wave beams is the main generation mechanism for the higher harmonics and the mean flow. In this section, the particular attention is paid on the second harmonic generation.

Each frequency can be differentiated by using the orthogonality relation. The second harmonic velocity vector is orthogonal to the terms that do not contribute to the generation; therefore, the mean energy equation can be obtained for the second harmonic wave beam separately. To derive separate energy equations for the second harmonic, the product of the conjugate of the second harmonic velocity vector ($\mathbf{u}^{*2\omega_0}$), and the momentum equation is calculated as

$$\langle \mathbf{u}^{*2\omega_0} \left(\frac{\partial \mathbf{u}}{\partial t} + \mathbf{N}(\mathbf{u}) \right) \rangle = -\frac{1}{\rho_0} \nabla p + \nu \nabla^2 \mathbf{u} + \mathbf{F}_g \rangle. \quad (55)$$

It is time-averaged over one primary frequency wave period. The full derivation of the non-linear operator is given in Appendix B. The conjugate of the second harmonic velocity vector only interacts with the quantities with the same frequency in time. Except for the non-linear terms, the conjugate of the second harmonic velocity vector only interacts with the terms induced by the second harmonic wave beam. Moreover, even though there is a gravitational term induced by the second harmonic wave, since the second harmonic velocity vector is out of phase with the second harmonic perturbation density, it still does not contribute to the mean energy flux equation of the second harmonic wave beam. As mentioned earlier, the main generation mechanism of the higher harmonics is the non-linear interaction between the incident internal wave beam and the reflecting internal wave beam. The leading order

term of the non-linear interactions obtained due to spatial gradients of the complex exponential part and its product with the conjugate of the second harmonic signal is the forcing term similar to the virtual forcing term in the incident internal wave beam energy. Finally, the mean kinetic energy equation for the second harmonic wave beam is obtained as

$$\begin{aligned} \frac{\partial \langle E_{2\omega_0}^k \rangle}{\partial t} + \nabla \cdot (\vec{C}g_{2\omega_0} \langle E_{2\omega_0} \rangle) \\ = -\frac{\nu N^2 k_x^2}{\omega^2} \langle E_{2\omega_0} \rangle - 2\epsilon^4 \rho_0 k_x A_{2\omega_0}^x A_{inc}^x A_{ref}^x \\ \times \sin(k_z^{2\omega_0} z - \phi_0). \end{aligned} \quad (56)$$

However, it is not enough to evaluate the total energy equation for the second harmonic signal. The complex conjugate of the perturbation density field for the second harmonic signal is multiplied with the energy equation and time averaged over one primary frequency signal period as follows:

$$\langle \frac{g^2}{2\rho_0 N_0^2} \rho^{*2\omega_0} \left(\frac{\partial \rho}{\partial t} + N_\rho(\rho, \mathbf{u}) \right) \rangle = w \frac{\rho_0}{g} N^2. \quad (57)$$

In the operation given in Eq. (57), the conjugate of the density perturbation field only interacts with the time derivative of the density perturbation field. The second harmonic velocity field is out of phase with the perturbation density field; therefore, the time-averaging cancels out. Moreover, as given in Appendix B, the non-linear term in the energy equation does not produce a signal with 2ω frequency; therefore, the product of the conjugate of the perturbation density field and the non-linear terms cancel out. Under these conditions, the mean available potential energy equation for the second harmonic wave beam can be given as

$$\frac{\partial \langle E_{2\omega_0}^p \rangle}{\partial t} = 0. \quad (58)$$

Therefore, the total energy equation can be obtained by adding Eqs. (58) and (56) as

$$\begin{aligned} \frac{\partial \langle E_{2\omega_0} \rangle}{\partial t} + \nabla \cdot (\vec{C}g_{2\omega_0} \langle E_{2\omega_0} \rangle) \\ = -\frac{\nu N^2 k_x^2}{\omega^2} \langle E_{2\omega_0} \rangle - 2\epsilon^4 \rho_0 k_x A_{2\omega_0}^x A_{inc}^x A_{ref}^x \\ \times \sin(k_z^{2\omega_0} z - \phi_0). \end{aligned} \quad (59)$$

In this present study, the steady-state response is analyzed by using the mean steady-state energy equation for the second harmonic wave which is given as

$$\begin{aligned} \nabla \cdot (\vec{C}g_{2\omega_0} \langle E_{2\omega_0} \rangle) = -\frac{\nu N^2 k_x^2}{\omega^2} \langle E_{2\omega_0} \rangle - 2\epsilon^4 \rho_0 k_x A_{2\omega_0}^x A_{inc}^x A_{ref}^x \\ \times \sin(k_z^{2\omega_0} z - \phi_0). \end{aligned} \quad (60)$$

The total time-averaged energy is again evenly distributed between the kinetic energy and the available potential energy; therefore, the total energy of the second harmonic can be given as

$$\begin{aligned} \langle E_{2\omega_0} \rangle = \epsilon^4 \frac{\rho_0}{2} \left(1 + \left(\frac{2k_x}{k_z^{2\omega_0}} \right)^2 \right) (A_{2\omega_0}^x)^2 \\ = \epsilon^4 \frac{\rho_0}{2} \frac{N_0^2}{\omega^2} \left(\frac{k_x}{k_z^{2\omega_0}} \right)^2 (A_{2\omega_0}^x)^2. \end{aligned} \quad (61)$$

A coordinate rotation can be performed to simplify Eq. (60) with the rotation angle $\theta_{2\omega_0} = \tan^{-1}(-2k_x/k_z^{2\omega_0})$. Similar to the incident internal wave beam, a new coordinate system $\xi_{2\omega_0} - \eta_{2\omega_0}$ is introduced. Note that r subscript stands for denoting reflection. Again, $\eta_{2\omega_0}$ is in the direction of the wave number vector $\vec{k}_{2\omega_0}$ and $\xi_{2\omega_0}$ is in the direction of the group velocity vector $\vec{C}g_{2\omega_0}$. Explicitly, the relation between the x - z coordinate system and $\xi_{2\omega_0} - \eta_{2\omega_0}$ coordinate system can be given as

$$\begin{bmatrix} \xi_{2\omega_0} \\ \eta_{2\omega_0} \end{bmatrix} = \begin{bmatrix} \cos \theta_{2\omega_0} & \sin \theta_{2\omega_0} \\ -\sin \theta_{2\omega_0} & \cos \theta_{2\omega_0} \end{bmatrix} \begin{bmatrix} x \\ z \end{bmatrix}. \quad (62)$$

Furthermore, the total energy equation can be simplified by substituting the definition of the second harmonic energy in Eq. (61). As a result, the following differential equation is obtained:

$$\begin{aligned} Cg_{2\omega_0}^{\xi_{2\omega_0}} \frac{\partial A_{2\omega_0}^x}{\partial \xi_{2\omega_0}} = -\frac{\nu N^2 k_x^2}{2\omega^2} A_{2\omega_0}^x - 2 \frac{(k_z^{2\omega_0} \omega)^2}{N_0^2 k_x} \\ \times A_{inc}^x A_{ref}^x \sin(k_z^{2\omega_0} z - \phi_0), \end{aligned} \quad (63)$$

where $Cg_{2\omega_0}^{\xi_{2\omega_0}} = \sqrt{\vec{C}g_{2\omega_0} \cdot \vec{C}g_{2\omega_0}}$. The analytical solution to Eq. (63) is given as

$$A_{2\omega_0}^x = \gamma_{2\omega_0} \exp(-\alpha_{2\omega_0} \xi_{2\omega_0}) \int \exp(\alpha_{2\omega_0} \xi_{2\omega_0}) F_{2\omega_0} d\xi_{2\omega_0}. \quad (64)$$

The integration of Eq. (64), coefficients $\gamma_{2\omega_0}$ and $\alpha_{2\omega_0}$ and the function $F_{2\omega_0}$ are given in Appendix C. Note that the integration limits are not given here, but they should cover the interaction region. As a result, the velocity field, the perturbation density field, and the perturbation pressure field for the second harmonic wave are obtained as

$$\begin{aligned} \mathbf{u}^{2\omega_0} = H_{2\omega_0} \exp(-\alpha_{2\omega_0} \xi_{2\omega_0}) \exp(\hat{\phi}(\eta_{2\omega_0})) \\ \times \sin(\hat{\phi}(\eta_{2\omega_0})) \cos \phi_{2\omega_0} (\vec{i}, -\frac{2k_x}{k_z^{2\omega_0}} \vec{k}), \end{aligned} \quad (65)$$

$$\begin{aligned} p^{2\omega_0} = \frac{\rho_0 N_0^2 H_{2\omega_0} Cg_{2\omega_0}^{\xi_{2\omega_0} k_x^2}}{(\omega k_z^{2\omega_0})^2} \exp(-\alpha_{2\omega_0} \xi_{2\omega_0}) \\ \times \exp(\hat{\phi}(\eta_{2\omega_0})) \sin(\hat{\phi}(\eta_{2\omega_0})) \cos \phi_{2\omega_0}, \end{aligned} \quad (66)$$

$$\begin{aligned} p^{2\omega_0} = \frac{2\rho_0 N_0^2 H_{2\omega_0} k_x}{g \omega k_z^{2\omega_0}} \exp(-\alpha_{2\omega_0} \xi_{2\omega_0}) \\ \times \exp(\hat{\phi}(\eta_{2\omega_0})) \sin(\hat{\phi}(\eta_{2\omega_0})) \sin \phi_{2\omega_0}. \end{aligned} \quad (67)$$

Similar to the primary frequency incident internal wave beam, the perturbation pressure field induced by the second harmonic wave can be associated with the velocity through the energy flux relation (14). Again similar to the primary incident internal wave beam, the perturbation density field is out of phase with the velocity field.

A. The second higher harmonic wave numerical solution

The analytical solution provided here is an approximate solution; it can also be verified by the numerical solution. The steady-state second harmonic mean energy equation is

given in Eq. (60). In the case of linear stratification, the group velocity is constant throughout the domain for a specific wave number vector and frequency. Therefore, the divergence of the energy flux can be reduced to the gradient of the energy multiplied with the group velocity vector. After expanding the time-averaged energy, the amplitude of the velocity in the x direction on the right-hand side of the equation drops out. Therefore, the resultant equation can be given as

$$\begin{aligned} Cg_{2\omega_0}^x \frac{\partial A_{2\omega_0}^x}{\partial x} + Cg_{2\omega_0}^z \frac{\partial A_{2\omega_0}^x}{\partial z} \\ = -\frac{\nu N^2 k_x^2}{2\omega^2} A_{2\omega_0}^x - 2 \frac{(k_z^{2\omega_0} \omega)^2}{N_0^2 k_x} A_{inc}^x A_{ref}^x \\ \times \sin(k_z^{2\omega_0} z - \phi_0). \end{aligned} \quad (68)$$

In the setting shown in Fig. 1, the second harmonic signal propagates downward. Therefore, the sign of the group velocity in the z direction is negative, whereas the sign of the group velocity in the x direction is positive. However, it may change in the case of oblique reflection, but the primary focus here is given in the case shown in Fig. 1. Moreover, the numerical method used here is the spectral collocation method. In terms of the grid choice, Gauss-Legendre-Lobatto points are assigned in both directions. This type of grid allows capturing a better resolution of the right hand side nearby the upper boundary where it has a more complicated spatial structure.

From a numerical analysis point of view, it is a first order partial differential equation. Thus it needs one boundary condition in each direction which should also respect the physics of the problem (Fig. 2). In the problem analysed here, the second harmonic signal propagates rightwards in the x direction and downwards in the z direction. Therefore, it should be compatible with boundary conditions. Therefore, no flux conditions are imposed at the top and the right boundaries. Furthermore, the first derivative in both the x and z directions can be written discretely and replaced in Eq. (68) which can be given discretely as

$$(Cg_{2\omega_0}^x \mathbf{D}_x + Cg_{2\omega_0}^z \mathbf{D}_z + \frac{\nu N^2 k_x^2}{2\omega^2}) A_{2\omega_0}^x = F_{2\omega_0}, \quad (69)$$

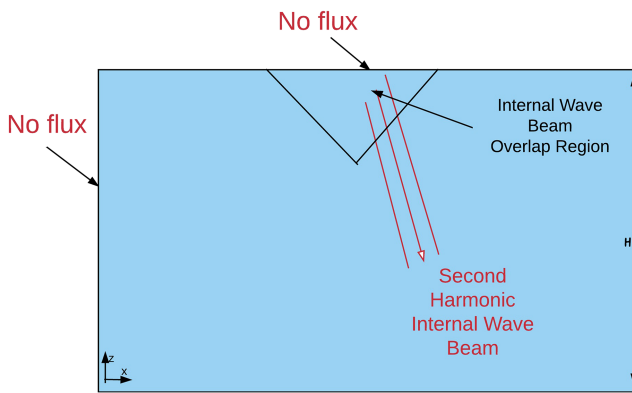


FIG. 2. Schematic of the second harmonic field generated by the nonlinear interaction between the incident and the reflecting internal wave beams. No flux conditions are imposed on the top boundary and the left boundary. However, no condition is imposed on the bottom and the right boundary.

where \mathbf{D}_x and \mathbf{D}_z are differentiation matrices in the x and z directions, respectively, and also $F_{2\omega_0}$ is the right-hand side forcing given in Eq. (68). The summation of the group velocities multiplied with differentiation matrices forms the resultant governing equation matrix; however, the top and the left boundary points are also included in this matrix. Therefore, the solution is given as

$$A_{2\omega_0}^x = (Cg_{2\omega_0}^x \mathbf{D}_x + Cg_{2\omega_0}^z \mathbf{D}_z + \frac{\nu N^2 k_x^2}{2\omega^2})^{-1} F_{2\omega_0}. \quad (70)$$

After obtaining the amplitude envelope $A_{2\omega_0}^x$, the perturbation density field and the perturbation pressure field can be obtained by the relations described in Sec. IV.

V. MEAN FLOW GENERATION DUE TO INCIDENT AND REFLECTING INTERNAL WAVE BEAM COLLISION

As shown in the previous work on the harmonic generation,¹⁷ the interaction between the incident internal wave beam and the reflecting internal wave beam produces the second harmonic signal 2ω and a mean flow. Differing from previous investigations done on the mean flow generation,^{17,23} here the mean flow generation is evaluated from the energy flux perspective. The velocity field, the perturbation pressure field, and the perturbation density field for the mean flow can be written in terms of fast and slow variables as

$$\epsilon^2 \mathbf{u}^0 = \epsilon^2 (u_x^0(X_0, Z_0, T, x, z) \vec{i}, u_z^0(X_0, Z_0, T, x, z) \vec{k}), \quad (71)$$

$$\epsilon^2 p^0 = \epsilon^2 p^0(X_0, Z_0, T, x, z), \quad (72)$$

$$\epsilon^2 \rho^0 = \epsilon^2 \rho^0(X_0, Z_0, T, x, z), \quad (73)$$

where $X_0 = \epsilon x$, $Z_0 = \epsilon z$, and $T = \epsilon^2 t$ are slow variables, and x and z are fast variables. In the case of mean flow, fast spatial variables are used to capture the spatial mean structure generated by the phase differences of the incident internal wave and the reflecting internal wave beam, whereas the slow variables take the amplitude interactions into account which are time-dependent during the transient period. Furthermore, a similar energy formulation can be used to derive the energy flow equation for the mean flow. As a result, the mean energy flow equation can be obtained for the mean flow separately as

$$\langle \mathbf{u}^0 (\frac{\partial \mathbf{u}}{\partial t} + \mathbf{N}(\mathbf{u})) = -\frac{1}{\rho_0} \nabla p + \nu \nabla^2 \mathbf{u} + \mathbf{F}_g \rangle. \quad (74)$$

After this operation, the mean energy flow equation is obtained as

$$\begin{aligned} \epsilon \frac{1}{2} \frac{\partial ((u_x^0)^2 + (u_z^0)^2)}{\partial t} + \epsilon \frac{1}{\rho_0} \nabla \cdot (p^0 \mathbf{u}^0) \\ = \epsilon^4 \frac{2u_z^0 k_x^2}{k_z} A_{inc}^x A_{ref}^x \sin(2k_z z + \phi_0) + \\ - \epsilon^4 2\nu (S_{ij}^0 S_{ij}^0) - \epsilon^4 \frac{1}{\rho_0} \rho^0 g u_z^0, \end{aligned} \quad (75)$$

where

$$S_{ij} = \begin{bmatrix} \frac{\partial u_x^0}{\partial x} & \frac{1}{2} (\frac{\partial u_x^0}{\partial z} + \frac{\partial u_z^0}{\partial x}) \\ \frac{1}{2} (\frac{\partial u_x^0}{\partial z} + \frac{\partial u_z^0}{\partial x}) & \frac{\partial u_z^0}{\partial z} \end{bmatrix}$$

is the strain rate tensor and its inner product with itself gives the viscous dissipation rate for the mean flow. Moreover, in case of mean flow, there is no polarization relation; therefore the buoyancy flux $\rho^0 g u_z^0$ is non-zero.

Differing from the propagating internal waves, in a mean flow field, the mean total energy is not evenly distributed between the kinetic energy and the available potential energy. As a result, the perturbation density field should be assessed separately as

$$\langle\langle \frac{\partial \rho}{\partial t} + N_\rho(\rho, \mathbf{u}) = w \frac{\rho_0}{g} N_0^2 \rangle\rangle, \quad (76)$$

where N_ρ is the non-linear operator given explicitly in [Appendix B](#). In addition, the time averaging operation given in Eq. (76) drops out the terms induced by the incident, the reflecting, and the second harmonic fields. Therefore, this time averaging operation results in the following relation:

$$\frac{\partial \rho^0}{\partial t} = -k_x (A_{inc}^x \varphi_{ref}^x + A_{ref}^x \varphi_{inc}^x) \cos(2k_z z + \phi_0) + u_z^0 \frac{\rho_0}{g} N_0^2. \quad (77)$$

Under these conditions, the steady-state response leads to the following equilibrium:

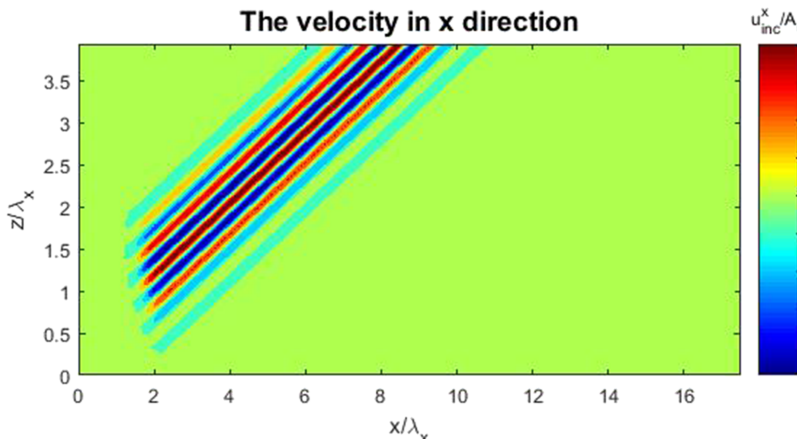
$$u_z^0 = \frac{2k_x^2}{\omega k_z} A_{inc}^x A_{ref}^x \cos(2k_z z + \phi_0). \quad (78)$$

Note that the perturbation density fields are given in terms of the velocity field amplitudes. In the beginning of the analysis, it is assumed that the incident internal wave beam, the reflecting internal wave beam, the second harmonic wave beam, and the mean flow satisfy the continuity condition separately. Therefore, the mean velocity field in the x direction is computed as

$$u_x^0 = - \int_0^x \frac{\partial u_z^0}{\partial z} dx'. \quad (79)$$

The derivative inside the integral (79) can be decomposed into slow and fast parts as it is done previously. The term $A_{inc}^x A_{ref}^x$ is governed by slow variables, and the cosine term $\cos(2k_z z + \phi_0)$ is governed by fast variables. Therefore, at leading order, the integral (79) can be given as

$$u_x^0 = \frac{4k_x^2}{\omega} \sin(2k_z z + \phi_0) \int_0^x A_{inc}^x A_{ref}^x dx'. \quad (80)$$



The mean velocity field is obtained within the interaction region between the incident and the reflecting internal wave beams. A similar type of mean flow structure is obtained with the previous studies on subsurface mean flow²³ which has the similar vertical cosine structure with half of the wave length in the z direction of the incident internal wave beam.

The analysis also shows that the stratification profile does not affect the mean flow directly, whereas it affects the generated higher harmonics via viscous dissipation. However, it indirectly affects the mean flow generation by amplifying the effects of viscous loss on the incident internal wave beam. Moreover, even though it flows outside that interaction region, it needs further analysis and most possibly an inner region and an outer region, where the effects of the interaction between the incident and the reflecting internal wave beams are negligible, matching is needed to obtain the mean velocity profile outside the interaction region. Additionally, the mean perturbation pressure field and the mean perturbation density field can also be obtained by solving Eq. (75) which also needs further investigation. In particular, the transient analysis of the mean perturbation density field should be done as it does not have a complex exponential multiplier so that it drops out in Eq. (77) when the system reaches the steady-state.

VI. RESULTS

In Secs. I–V, the analysis is performed for both linear and non-linear physics. The linear physics govern the propagation of the incident internal wave beam generated by the virtual forcing pedal which mimics the generation mechanism in nature. Moreover, the energy transfer from the incident internal wave beam to the reflecting internal wave beam is also governed by linear theory. However, the second harmonic and the mean flow are generated by the non-linear interaction between the incident internal wave beam and the reflecting internal wave beam.

A. Linear effects

1. The incident internal wave beam generation

First, the incident internal wave beam is obtained by solving Eqs. (3) and (4); it is also an exact solution to the non-linear

FIG. 3. The incident velocity field in the x direction for $\theta = 23^\circ$.

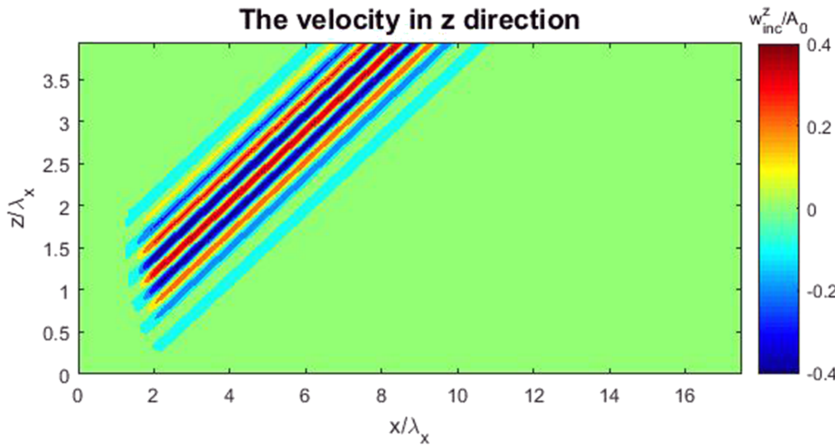


FIG. 4. The incident velocity field in the z direction for $\theta = 23^\circ$.

Navier-Stokes equations under the Boussinesq approximation at the leading order where the rate of change in amplitude is much slower than the rate of change in phase. As explained in Sec. II, the amplitude of the incident internal wave beam is governed by slow variables in space and time.

Initially, the energy is transferred to the incident internal wave beam from the virtual forcing pedal, and the energy flux of the incident internal wave beam reaches the peak energy at the point $\xi = 2\sqrt{2}\sigma + \alpha\sigma^2$ as shown in Fig. 3. The virtual forcing pedal has a Gaussian shape which leads to an error function type of profile along the ray path direction. However, it is just an approximation; they are either generated by the turbulent wake¹⁸ or internal tides⁷ in a stratified ocean. A sample incident velocity profile is given in Figs. 4 and 5. They are also similar to the velocity field obtained in previous studies.^{5,14}

2. Viscous decay

After an internal wave beam leaves the virtual forcing region, it propagates towards the free slip surface. It attenuates exponentially along the ray path as shown previously.¹² The rate of exponential decay is dependent on the α parameter which explicitly shows how the viscous dissipation is dependent on certain parameters. It shows that it is quadratically amplified by the increase in k_x ; the larger wave number leads to steeper gradients in velocity profile which physically leads to higher viscous loss along the ray path. Finally,

the energy flux is integrated along the wave number direction to obtain the total flux in the group velocity direction as follows:

$$\begin{aligned} F_{total}(\xi) &= \int_{-\infty}^{\infty} \langle E \rangle C g_{\xi} d\eta = \epsilon^2 \rho_0 C g_{\xi} \frac{(A_0 N_0 k_x)^2}{(\omega^2 k_z)^2} \\ &\quad \times \exp(-2\alpha\xi) \int_{-\infty}^{\infty} \exp(-\frac{\eta^2}{\sigma^2}) d\eta \\ &= \epsilon^2 \sqrt{\pi} \rho_0 C g_{\xi} \sigma \frac{(A_0 N_0 k_x)^2}{(\omega^2 k_z)^2} \exp(-2\alpha\xi). \end{aligned} \quad (81)$$

In Fig. 3, the energy flux is normalized with respect to the maximum energy flux $F_{max} = \epsilon^2 \sqrt{\pi} \rho_0 C g_{\xi} \sigma (A_0 N_0 k_x)^2 / (\omega^2 k_z)^2$. It is achieved at $\xi = 2\sqrt{2}\sigma + \alpha\sigma^2$.

The energetics results of the incident internal wave beam for various stratification and angle of incidence is provided in Table I. The results are presented in decreasing angle of incidences $\theta = 25^\circ, 20^\circ, 15^\circ, 10^\circ$, while the wave number in the x direction is held constant. There is a significant increase in viscous loss as the angle of incidence decreases as the wave number in the z direction increases. The wave number in the x direction is deliberately held constant in each angle of incidence; the lower angle of incidence leads to a larger wave number in the z direction. Therefore, the vertical spatial structure experiences higher viscous loss. Here, it is evaluated in different cases. However, the varying angle of propagation can be observed in non-uniform stratifications.

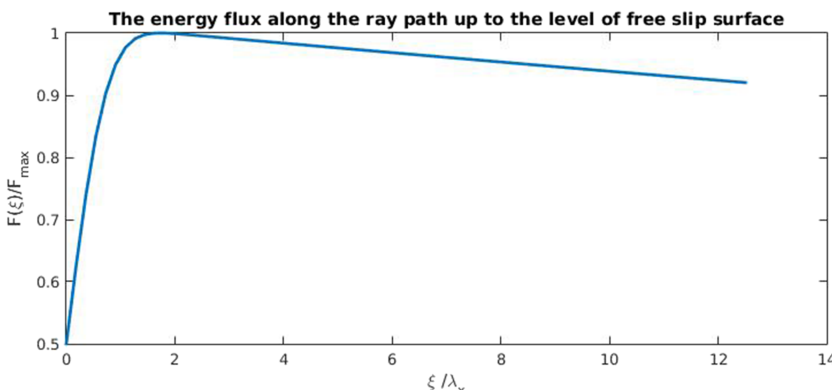


FIG. 5. Plot of energy flux of the incident internal wave beam along the ray path. The ray path start from the center of excitation and it ends when the ray path at the center line of the internal wave beam reaches the free slip surface.

TABLE I. The energetics results of the incident internal beam under various buoyancy frequencies and wave numbers.^{a,b}

ω/N_0	$k_x (\text{m}^{-1})$	σk_η	θ	$\alpha (\text{m}^{-1})$	ξ_H/λ_x	$F(\xi_H)/F_{\max}$
0.466	7.17	7.02	25°	6.52×10^{-4}	7.94	0.992
0.466	7.17	7.02	25°	6.52×10^{-3}	7.94	0.921
0.466	14.34	14.04	25°	1.04×10^{-2}	7.94	0.942
0.466	14.34	14.04	25°	0.104	7.94	0.546
0.363	7.17	8.41	20°	1.59×10^{-3}	8.26	0.978
0.363	7.17	8.41	20°	1.59×10^{-2}	8.26	0.810
0.363	14.34	16.82	20°	1.59×10^{-2}	8.26	0.859
0.363	14.34	16.82	20°	0.255	8.26	0.207
0.267	7.17	11.11	15°	5.1×10^{-3}	8.23	0.935
0.267	7.17	11.11	15°	5.1×10^{-2}	8.23	0.509
0.267	14.34	22.22	15°	8.16×10^{-2}	8.23	0.609
0.267	14.34	22.22	15°	1.59×10^{-3}	8.23	6.4×10^{-3}
0.176	7.17	16.57	10°	2.52×10^{-2}	7.95	0.720
0.176	7.17	16.57	10°	0.252	7.95	3.57×10^{-2}
0.176	14.34	33.14	10°	0.414	7.95	8.41×10^{-2}
0.176	14.34	33.14	10°	4.14	7.95	0

^a k_η is the magnitude of the wave number vector.

^b ξ_H is the coordinate of the centreline at the surface level.

Finally, the result shows that the stronger buoyancy frequency leads to stronger viscous loss. In real oceanic conditions, the density is not linearly stratified. It has a well-mixed region on the top and a localized high density gradient region called pycnocline under that well-mixed region. Under the pycnocline region, it is assumed to be linearly stratified.^{5,20} This quadratic dependence implies that the effect of viscous dissipation is felt much stronger around the pycnocline region compared to the lower layer. Therefore, the inviscid energetics analysis may not give accurate results. Further investigations are required to quantify

the amount of viscous dissipation around the pycnocline region.

3. Internal wave beam reflection from free slip surface

The reflecting internal wave beam is obtained to satisfy the free slip surface condition which requires no flux at the top boundary. It requires both phase matching and the amplitude matching of the reflecting internal wave beam. The spatial structure of the incident and the reflecting internal wave beams is similar to the ones obtained in previous studies^{2,14} as shown in Fig. 6. The amplitude of the incident internal wave beam diminishes as it attenuates viscously. Therefore, the viscous loss directly affects the amplitude of the reflecting internal wave beam.

In addition, the phase matching is also important in a way that it determines the wave number and the frequency of the reflecting internal wave beam. The frequency sets the angle of propagation of the reflecting internal wave beam. Furthermore, these quantities also determine the fate of the reflecting internal wave beam as they affect the viscous loss parameter α which is same for both the incident and the reflecting internal wave beams.

B. Non-linear effects

1. The second harmonic generation

The non-linear interaction between the incident internal wave beam and the reflecting internal wave beam generates two different forcing fields. One of them has a frequency 2ω and the mean flow structure in space. It is also shown by previous studies.^{16,17} The non-linear forcing field with a frequency 2ω generates the second harmonic wave and its magnitude is on the order of the incident internal wave beam amplitudes

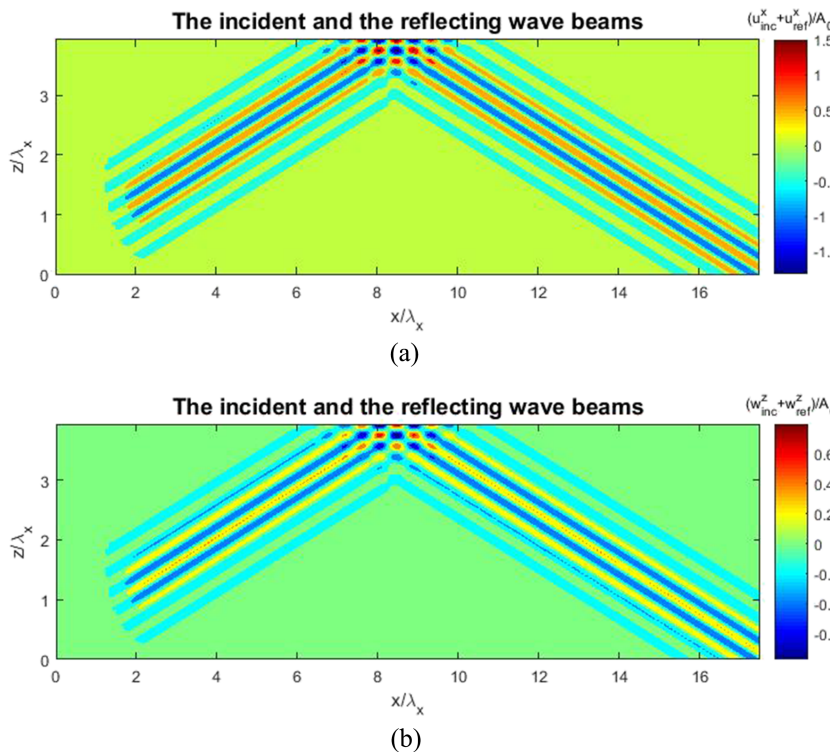
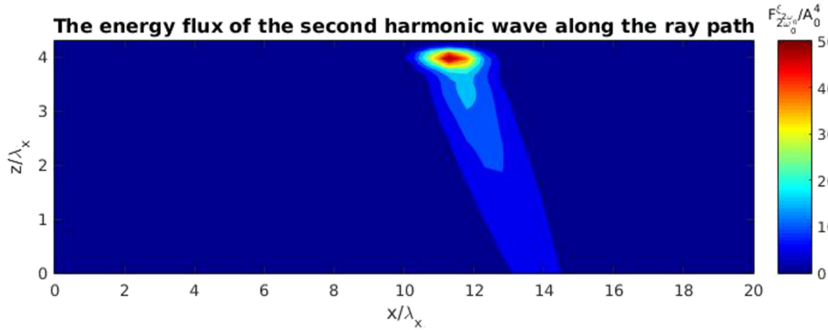


FIG. 6. The velocity fields of the incident and the reflecting internal wave beams in the x direction and z direction for $\theta = 23^\circ$.



square $O(A^2)$. Therefore, this forcing field results in the second harmonic wave field with the amplitude on $O(A^2)$.

As shown in Eqs. (56) and (58), the non-linear forcing of the second harmonic wave appears in the momentum equation and it contributes to the kinetic energy. However, there is no non-linear contribution to the available potential energy of the second harmonic wave. Nonetheless, independent of the source of the contribution, the total energy is again evenly distributed between the kinetic energy and the available potential energy. Because of this, Eqs. (56) and (58) are added, then Eq. (59), which governs the total mean energy flux of the second harmonic wave, is obtained.

Even though Eq. (59) can be used to obtain a transient solution, in the present study, the attention is paid on the steady-state solution. After obtaining a solution to Eq. (60), the rest of the quantities such as the total velocity field, the perturbation density field, and the perturbation density field can be written in terms of the velocity field. Furthermore, the right-hand side forcing of Eq. (60) is the product of A_{inc}^x and A_{ref}^x multiplied with a sinusoidal structure with a wave number $k_z^{2\omega_0}$ in vertical as shown in Fig. 7. The sinusoidal multiplier appeared due to the following inner product in Eq. (59):

$$\text{Re}\left(\frac{\omega}{2\pi} \int_{2\pi/\omega+t'}^{t'} -ie^{i(\phi_{inc}+\phi_{ref}-\phi_{2\omega_0})t} dt\right) = \sin(k_z^{2\omega_0} z - \phi_0). \quad (82)$$

In this paper, the wave number of the second harmonic field is chosen similar to the previous study¹⁷ which assumes the wave number of the second wave in the x direction is twice of the incident internal wave beam's wave number in the x direction; therefore, $k_x^{2\omega_0} = 2k_x$. The group velocity

FIG. 7. The energy flux of the second harmonic wave for $\theta = 25^\circ$. It is obtained numerically by solving Eq. (81) on a Legendre-Gauss-Lobatto grid in both the x and z directions where the number points in the z direction $N_z = 40$ and the number of points in the x direction $N_x = 40$. It is also normalized with respect to the fourth power of A_0 which is indeed the order of the second harmonic energy flux.

direction is orthogonal to the wave number direction which appears explicitly in Eq. (60). Furthermore, the group velocity direction also determines how much energy is transferred from the non-linear forcing region to the second harmonic wave. Due to the sinusoidal structure, depending on the direction of propagation, the non-linear forcing region either gives energy to the second harmonic wave or take energy from it. The total energy transferred to the second harmonic wave is highly dependent on the sinusoidal vertical structure of the non-linear forcing field.

The generation mechanism is one aspect of the problem analysed here. The fate of the second harmonic wave is also another issue to be addressed. As stated in Sec. IV, a necessary condition for the generation of propagating second harmonic wave is that $2\omega < N$; if this condition is not satisfied, the non-linear forcing field generates an evanescent second harmonic wave field as shown numerically by Zhou and Diamessis.²³ It restricts the main attention to $\theta < 30^\circ$ for the incident internal wave beams propagation angle. Moreover, in the case of $\theta < 30^\circ$, the stratification is still an effective parameter on the fate of the second harmonic wave. As mentioned earlier, the stratification also affects the viscous dissipation. Similarly, the stratification determines the wave number vector via the dispersion relation, which directly affects the magnitude and the direction of the spatial gradients of the velocity profile. As known, the larger spatial gradients in the velocity profile leads to higher viscous loss. Therefore, it directly affects the energetics of the second harmonic wave along its direction of propagation. As a result, the second harmonic wave decays viscously along the ray path shown in Fig. 8. Furthermore, the exact amount of energy transferred to the

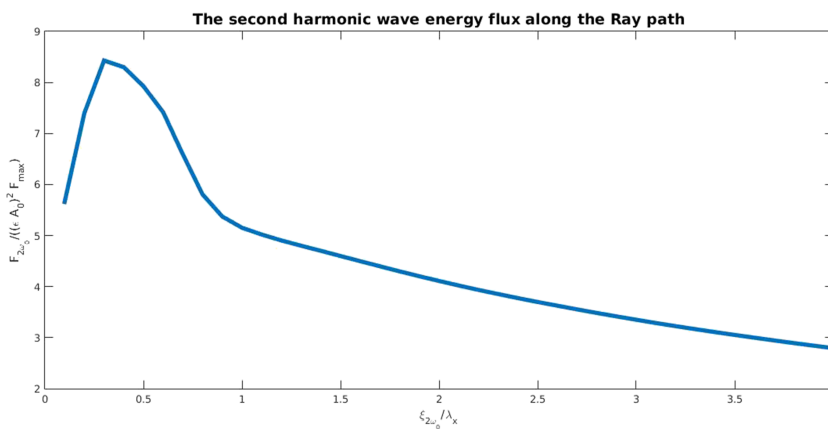


FIG. 8. The integrated energy flux of the second harmonic wave for $\theta = 25^\circ$. It is obtained via numerical integration along the wave number direction. The integration limits are determined so that it captures all of the energy. It is also normalized with respect to the fourth power of A_0 which is also the order of the second harmonic energy flux integral. An energy flux peak and then a sharp decay can be observed due to the spatial structure of the non-linear forcing region.

second harmonic wave is quantified by integrating the energy flux of it along the wave number direction as

$$F_{total}^{2\omega_0} = \int_{-\infty}^{\infty} C g_{2\omega_0}^{\xi_{2\omega_0}} \langle E_{2\omega_0} \rangle d\eta_{2\omega_0}. \quad (83)$$

The energy flux of the second harmonic wave is normalized with respect to A_0^4 rather than the energy flux of the incident internal energy flux which is more meaningful in terms of scaling. As it is directly proportional to A_0^4 , for different incident internal wave beam amplitudes the ratio of the energy fluxes changes; however, $F_{total}^{2\omega_0}/A_0^4$ is constant.

In Fig. 9, it can be seen that the energy flux reaches its peak around $0.5\lambda_x$ distance from the reference point which is the centreline of the reflection point. However, after that peak, it rapidly decays. This decay is caused by the energy withdrawal due to the non-linear forcing region. The vertical spatial structure has a sinusoidal distribution as shown in Fig. 7. As a result of this, if the amplitude of the second harmonic velocity field is positive and the non-linear forcing field in Eq. (60) is positive, the amplitude increases. At the same time, if the sign of the non-linear forcing field and the amplitude of the second harmonic wave at a given location are different, the non-linear forcing field draws energy from the second harmonic wave. As a result, it causes a sharp increase and a sudden decrease in energy flux as shown in Fig. 9.

After the second harmonic wave propagates outside of the non-linear forcing region, it shows viscous decay which is exponential with a slope $\alpha_{2\omega}$ given in Appendix C. The effective non-linear forcing region roughly ends at $\xi_{2\omega_0} = \lambda_x$ in Fig. 9. Therefore, the analytical solution to the second harmonic wave is valid after $\xi_{2\omega_0} > \lambda_x$. More it also means that the second harmonic wave preserves its structure along the wave number direction which is given analytically in Appendix C. The amplitude profile of the velocity field in the x direction for $\theta = 25^\circ$ is given in Fig. 10. It can be observed that the profile is not purely Gaussian, but it is modified with a

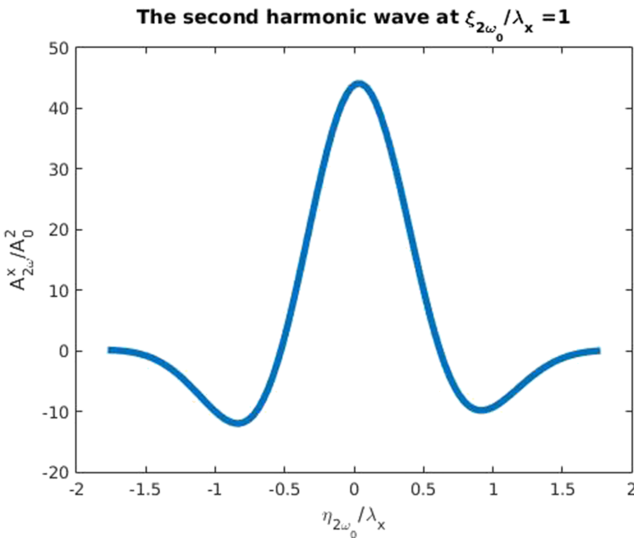


FIG. 9. The amplitude of the second harmonic velocity field in the x direction for $\theta = 25^\circ$ obtained analytically after the non-linear forcing region. It is also normalized with respect to the second power of A_0 which is the order of the second harmonic wave in the x direction.

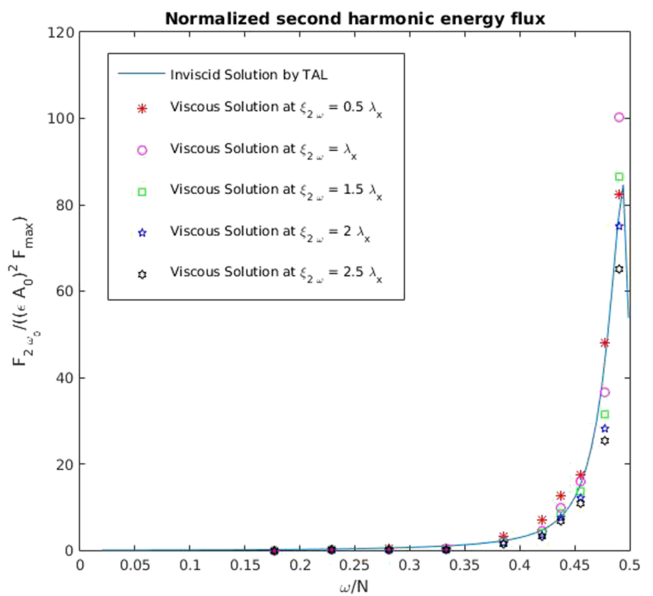


FIG. 10. The normalized second harmonic energy flux computed by both the inviscid analytical solution and the viscous analytical solution for $\theta \in [0^\circ, 30^\circ]$.

sinusoidal structure. It is the consequence of the spatial structure of the non-linear forcing region which was translated as a profile along the ray path via group velocities. It can be seen in the analytical solution for the second harmonic wave field.

As a result, it can be said that the vertical sinusoidal structure with the wave number $k_z^{2\omega_0}$ affects both how the energy is transferred to the second harmonic wave and also determines the amplitude profile along the wave number direction. In that context, the vertical profile of the non-linear forcing is also determined by the angle of incidence and the magnitude of the wave number. Some results for various angles $\theta \in [25^\circ, 20^\circ, 15^\circ, 10^\circ]$ are presented in Table II. Moreover, in Table II, the results for different wave numbers at the same angle of incidence are also presented to observe the effect of the magnitude of the wave number in terms of the energy transfer to the second harmonic wave.

Finally, the results show that the peak energy flux is magnified by the increasing incident wave number for $\theta \in [25^\circ, 20^\circ]$. In Eq. (76), the non-linear forcing is composed of the multiplication of the incident amplitude and the reflecting amplitude and $2(k_z^{2\omega_0} \omega)^2 / N_0^2 k_x$ factor. The factor multiplying the amplitude product increases as the incident wave number increases for the same angle of incidence. Therefore, it increases the peak energy transfer to the second harmonic wave. However, it also increases the wave number of the second harmonic wave which also leads to higher viscous loss after the second harmonic wave leaves the non-linear forcing region. The results for $\theta \in [25^\circ, 20^\circ]$ also confirms this finding. However, in the cases where $\theta \in [15^\circ, 10^\circ]$, the increase in the magnitude of the wave number does not increase the peak energy transfer and also increases viscous dissipation after the second harmonic wave leaves the non-linear forcing region. The main reason is that the higher wave number also increases the viscous loss along the ray path of the incident internal wave beam. In these cases, this viscous loss diminishes the

TABLE II. The energetics results of the second harmonic wave field induced by the collision of the incident internal wave beam field and the reflecting internal wave field for various angles of incidence and wave numbers.^{a,b}

ω/N_0	$k_x (\text{m}^{-1})$	σk_η	$\alpha (\text{m}^{-1})$	ξ_H/λ_x	$F(\xi_H)/F_{max}$	$\bar{F}_{2\omega_0}(0.5\lambda_x)$	$\bar{F}_{2\omega_0}(\lambda_x)$	$\bar{F}_{2\omega_0}(1.5\lambda_x)$
0.466	7.17	7.02	6.52×10^{-4}	7.94	0.992	54.31	50.2	42.74
0.466	14.34	14.04	1.04×10^{-2}	7.94	0.942	107.2	43.84	20.91
0.363	7.17	8.41	1.59×10^{-3}	8.26	0.978	4.015	2.513	2.16
0.363	14.34	16.82	1.59×10^{-2}	8.26	0.859	4.595	2.366	1.663
0.267	7.17	11.11	5.1×10^{-3}	8.23	0.935	0.5475	0.4269	0.3389
0.267	14.34	22.22	8.16×10^{-2}	8.23	0.609	0.259	0.1037	0.06552
0.176	7.17	16.57	2.52×10^{-2}	7.95	0.720	0.1268	0.1005	0.09153
0.176	14.34	33.14	0.414	7.95	8.41×10^{-2}	8.1×10^{-3}	5.5×10^{-3}	4.4×10^{-3}

^aThe energy flux of the second harmonic is on the order of A_0^4 ; therefore, it is normalized with respect to A_0^4 and denotes as $F(\xi_{2\omega_0})/A_0^4 = \bar{F}_{2\omega_0}(\xi_{2\omega_0})$.

^bThe energy fluxes are sampled at $\xi_{2\omega_0} = 0.5\lambda_x, \lambda_x, 1.5\lambda_x$.

amplitude of the incident internal wave beam so that the increase in the factor multiplying the amplitude product cannot compensate the decrease in the non-linear forcing. Therefore the peak energy flux also decreases. Moreover, it also increases the viscous dissipation of the second harmonic wave. In addition to the magnitude of the incident wave number, the angle of incidence significantly affects the energy transfer to the second harmonic wave. The results in Table II clearly show that as the angle of incidence which is less than 30° decreases the amount of energy transferred to the second harmonic wave also decreases. Energy transmission to the second harmonic reaches its peak around $\theta \approx 29^\circ$ and it decreases significantly as the angle of incidence decreases as found by Tabaei *et al.*¹⁷ The results are compared with the inviscid analysis by TAL which is solved in Appendix D for the inviscid incident internal wave beam profile derived here. Finally, the energy flux is normalized with respect to the incident energy flux as follows:

$$F_{21} = \frac{4\pi N_0 \rho_0 \cos \gamma_2 \int_0^\infty k_x |A_2(k_x)|^2 dk_x}{A_0^2 F_{max}}. \quad (84)$$

The main reason to observe such pattern is the vertical sinusoidal structure and the group velocity direction. As the angle between the incident and the reflecting internal wave beams decreases, the vertical sinusoidal structure of non-linear forcing gets finer. As the second harmonic wave

propagates along the group velocity direction, it either draws energy or gives energy to the non-linear forcing region depending on the sign of the non-linear forcing region. The finer scale vertical structure leads to less energy transfer to the second harmonic wave as it changes its energetics character more frequently along the ray path. The non-linear forcing regions for $\theta = 25^\circ$ and $\theta = 20^\circ$ are plotted in Figs. 11 and 12, respectively. These figures show that as the angle of incidence decreases, the vertical structure gets finer. As a result, it leads to a lower rate of energy transfer to the second harmonic wave.

In this study, the main focus is given on the interaction between the incident and the reflecting internal wave beams. However, these results can be extended to any other internal wave beam collision. As the angle between the interaction, internal wave beams with the same frequency decreases the energy transfer to the second harmonics decreases due to the finer scale sinusoidal structure along the ray path of the second harmonic wave.

2. Mean flow generation

Upon the interaction between the incident and the reflecting internal wave beams, depending on the angle, a propagating or an evanescent second harmonic wave is generated. However, the mean flow is generated in every angle of incidence.

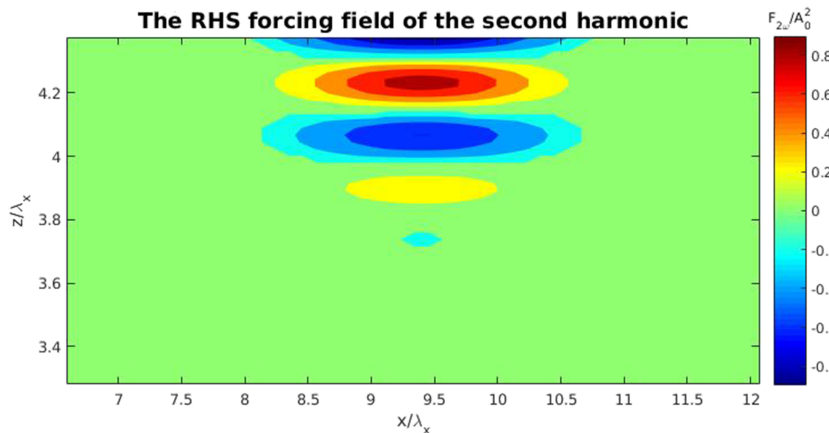
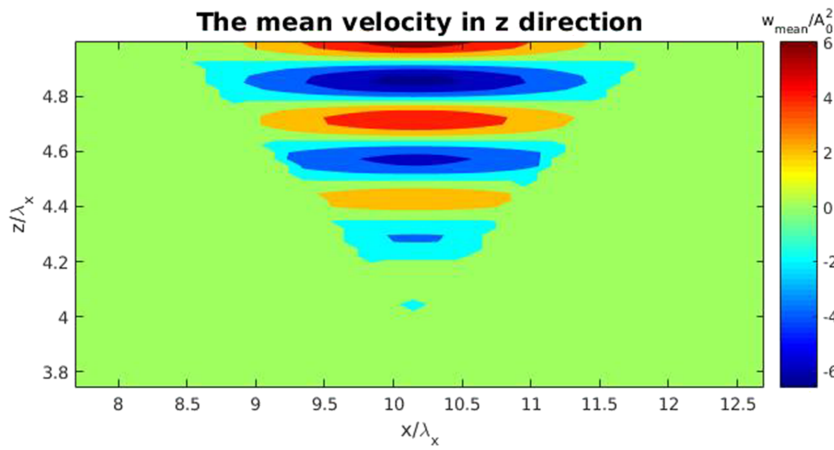
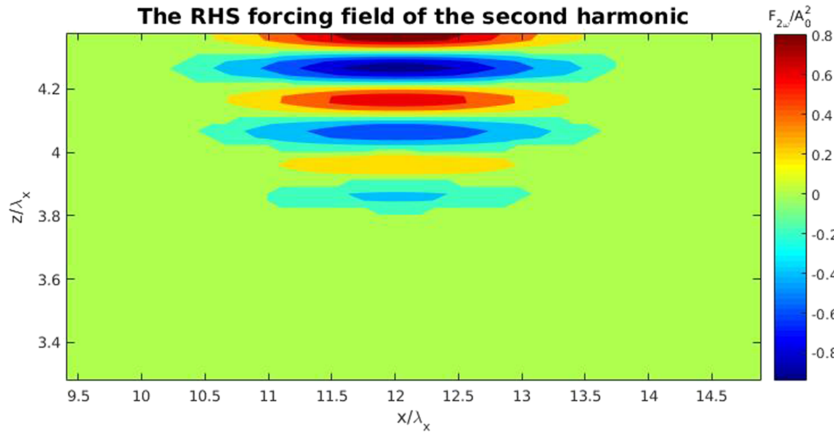


FIG. 11. The non-linear forcing region normalized with A_0^2 for the angle of incidence $\theta = 25^\circ$.



It is found to be locally confined in a previous analysis.^{17,23} The same result is also obtained here; the mean velocity in the z direction is obtained by the energy equation (77) where the mean velocity in the z direction balances the non-linear forcing term generated by the interaction in Eq. (77). By the continuity equation, the mean velocity in the x direction is also obtained in Eq. (80).

The generation mechanism of the mean flow is similar to the second harmonic signal. However, the mean perturbation pressure and the perturbation density cannot be found by phase relations as it is done for the second harmonic wave. In the

FIG. 12. The non-linear forcing region normalized with A_0^2 for the angle of incidence $\theta = 20^\circ$.

present study here, only the mean velocity field is obtained. Even though the energy flux equation (76) is derived, it is not solved explicitly. The solution of Eq. (76) will give an insight into the fate of mean flow outside of the interaction region. Despite the lack of an explicit solution to Eq. (76), some interpretations can be made about the fate of the mean flow. First, differing from the propagation second harmonic wave, the viscous dissipation of the mean flow is independent of the stratification. However, the generation of the mean flow is dependent on the amplitude of the incident internal wave beam which is affected by the stratification profile viscously.

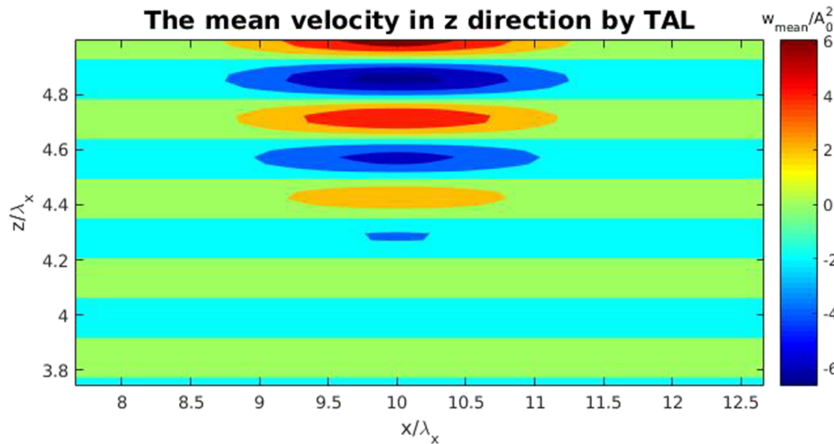


FIG. 14. The mean velocity in the z direction normalized with A_0^2 for the angle of incidence $\theta = 30^\circ$ obtained by the inviscid solution.

In the case of a non-linear stratification profile such as pycnocline, mean flow's independence of the stratification profile after generation may enable it to survive further inside than the second harmonic wave. However, it needs further analysis as this phenomenon will be highly dependent on the strength of the pycnocline.

The mean velocity profile obtained here is similar to the recent work by Zhou and Diamessis,²³ where they obtained a same vertical sinusoidal vertical structure with a wave number $2k_z$, as shown in Figs. 13 and 14. Moreover, in this study, differing from the analytical solution proposed there, the viscous effects of the incident internal wave beam is considered. The viscous dissipation of the mean flow considered here adds $O(A^2)$ effects as it directly diminishes the amplitude of the mean flow which is also $O(A^2)$. In a previous study,²³ it was also shown that the mean flow induced by the incident and reflecting internal wave interaction does not lead to Richardson Number $Ri < 1/4$; therefore, it does not cause instability. Here this issue is not addressed.

VII. DISCUSSION

Internal waves are generated by turbulent wakes¹⁸ or internal tides interacting with topography,⁷ however, in simulations,^{14,23} it is replaced with the virtual forcing pedal given in [Appendix A](#). This forcing pedal can generate an internal wave beam with a single wave number vector and smooth profile differing from generation mechanisms in nature; this makes analysis much simpler.

In the energy formulation given here, the inner product of the momentum equation and the conjugate of the incident internal wave velocity field and the inner product of the energy equation and the incident internal wave perturbation density field are taken and added to form a single mean energy propagation equation for the incident internal wave beam. This formulation is based on the assumption that the relation between the velocity field and the perturbation density and the perturbation pressure fields are determined by the fast phase variables in the complex exponential. However, the evolution of the amplitude is determined by slow variables.

After generation, the incident internal wave beam propagates along the ray path up to the free slip surface; it attenuates due to viscous dissipation which is quadratically dependent on the buoyancy frequency of the background and the wave number k_x . This viscous dissipation also determines how much energy is transferred to the reflecting internal wave beam. The free slip surface imposes no flux condition at the free slip surface; this condition enables to determine both the amplitude and the phase of the reflecting internal wave beam. Differing from the previous analysis,¹⁷ the group velocities of the reflecting internal wave beam explicitly appear. Therefore there is no need to impose radiation conditions.

After reflection, the incident and the reflecting internal wave beams interact non-linearly and generate the second harmonic wave and the mean flow. Even though the incident internal wave beam and the reflecting wave beam are exact non-linear solutions, the non-linear interaction terms generate

a non-linear forcing term for both with a frequency double of the incident internal wave beam's frequency and mean spatial forcing structure in the interaction region where they collide.

First, the non-linear forcing term with a frequency 2ω may generate either a propagating or evanescent second harmonic wave. It is directly dependent on the buoyancy frequency of the background stratification. If $2\omega > N_0$, then the second harmonic wave is evanescent, else a propagating internal wave beam can be generated. This condition restricts the angles of incidence $\theta < 30^\circ$ for the generation of the propagating second harmonic wave. Even in the case of propagating second harmonic wave, the amount of energy transferred is highly dependent on the angle of incidence. The results show that the energy transferred to the second harmonic wave diminishes, as the angle of incidence decreases. The main physical mechanism behind this type of trend in energy transfer to the second harmonic can be summarized as follows. The lower angle of incidence creates a finer sinusoidal structure along the ray path of the second harmonic wave as shown in Figs. 11 and 12. As it changes sign quickly in the region where the non-linear forcing is highest, the non-linear forcing regions start drawing energy from the second harmonic wave rather than doing work on it in regions where the non-linear forcing term is negative; therefore, it loses energy more frequently in that region. The sharp decay in energy flux of the harmonic due to the negative forcing region is shown in Fig. 8.

Additionally, even though the viscosity is also effective in the interaction region, it is not as effective as the negative forcing regions. However, the viscous effects become dominant after the second harmonic wave propagates outside of the non-linear forcing region. Again in Fig. 8, it can be observed that the energy loss occurs due to viscosity after $\xi_{2\omega_0} > \lambda_x$. The analytical solution provided in [Appendix C](#) is also valid after the non-linear interaction region. The analytical solution also shows that the cross beam amplitude profile is also dependent on the vertical sinusoidal structure of the non-linear forcing region. This vertical profile is translated along the ray path via group velocities hence the amplitude profile is obtained in Fig. 10.

Another consequence of the non-linear interaction is the mean flow in the subsurface region. This problem is also addressed in previous studies.^{17,23} The vertical structure obtained here is also same with the previous studies. In addition, the effect of viscosity is also considered in this paper. Even though the viscous effects do not appear explicitly, these affect the mean profile via the energy dissipation along the ray path of the incident internal wave beam. As a direct consequence of it, the energy transferred to the reflecting internal wave beam also diminishes. As a result of it, it modifies the mean flow profile in $O(A^2)$.

The non-linear forcing term does not produce single wave number but a spectrum of wave number for frequency 2ω . However, the energy integration provided in [Appendix C](#) results in negligible amount of energy transfer to most of the spectra of the wave numbers due to the sinusoidal forcing structure in the interaction region as shown in Fig. 12. The further analysis should be done to identify the wave number of the

second harmonic wave which maximizes the energy transfer from the non-linear forcing region to the second harmonic wave along the direction of propagation. The similar analysis for the higher harmonics generation in 3-D can be done. The energy formulation given in Eq. (60) can be directly extended to 3-D setting. Nonetheless, the non-linear interaction terms should be re-calculated for three dimensional internal wave beam collision. Moreover, the non-linear forcing term that would be obtained in 3-D setting would not produce discrete directions of the second harmonic wave propagation but a 3-D spectrum of wave number for 2ω frequency, but for most of the spectra, the energy transfer to the higher harmonics would be again negligible for the same argument. This analysis deserves further investigation.

The analysis presented here is focused on small amplitude internal waves. In a regular perturbation approach, it creates the non-linear forcing terms with different orders of magnitudes. The main idea is to match the terms in the same order. However, the formulation in Eqs. (70) and (73) also proposes frequency matching by using the functional orthogonality of the complex exponential functions of the terms with different frequencies. Moreover, the inner product formulation would separate terms with different frequencies if the time scale of the amplitude of internal wave beams is much slower than the time scale of the complex exponential. This functional orthogonality property would allow formulating the higher harmonic generation problem for finite amplitude cases. In the case of finite amplitude formulation, the separate equation for each frequency would again be obtained by the similar energy formulation, but the order matching would not be used. Moreover, the interaction between the incident internal wave beam and the second harmonic would produce a non-linear forcing term with frequency ω which will have a non-negligible effect on the incident and the reflection internal wave beams. Finally, for the finite amplitude case, the problem would be given as a non-linear dynamical system which governs the amplitude evolution of each frequency as long as the scales of the amplitude and the complex exponential terms obey the functional orthogonality condition.

Lastly, the resultant governing equation (60) can also be extended to non-linear stratifications. However, even though the linear effects of non-linear stratifications can be felt in Eq. (74), the non-linear effects of the internal wave beam refraction should also be considered in the extension of this formulation to the possible non-linear stratification problem. The linear effects of the non-linear stratification include linear refraction of the internal wave beam and the variable viscous dissipation rate. First, the linear refraction would lead to changes in both directions and the magnitude of the group velocity. The change in magnitude of the group velocity would lead to either energy accumulation of an internal wave beam in a certain level or energy diminution of it. Furthermore, the viscous dissipation term is quadratically dependent on the buoyancy frequency. If the slow variable assumption is still valid, Eq. (60) can be left as it is. Nonetheless, the existing models^{5,20} are inviscid; it may not be valid in non-linear stratification problems such as the pycnocline model which is a more realistic representation of oceans. In the case of pycnocline, the buoyancy frequency around the pycnocline may

reach 10 times more than that of the lower layer. As a result, it would lead to non-negligible viscous loss around the pycnocline region. In this way, the model proposed here may capture this viscous effect around the pycnocline if it is modified accordingly.

ACKNOWLEDGMENTS

I would like to thank Tubitak Space Technologies Research Institute for supporting this work.

APPENDIX A: VIRTUAL FORCING PEDAL

The same formulation with Zhou and Diamessis²³ for the virtual forcing pedal is used,

$$F_u = \frac{U_f}{T} \left(F \frac{k_z}{k_x} \cos \phi - \frac{\partial F}{\partial z} \frac{1}{k_x} \sin \phi + \frac{\partial F}{\partial x} \frac{k_z}{k_x^2} \sin \phi \right), \quad (A1)$$

$$F_w = \frac{U_f}{T} F \cos \phi, \quad (A2)$$

$$F_\rho = - \left| \frac{d\bar{\rho}}{dz} \right| \frac{U_f}{\omega_0 T} F \sin \phi, \quad (A3)$$

where $\phi = k_x x - k_z z - \omega_0 t$, U_f is the reference velocity scale, and T is the wave period and the Gaussian forcing region is

$$F(x, z) = \exp \left[-\frac{(x - x_{cen})^2}{2\sigma_x^2} - \frac{(z - z_{cen})^2}{2\sigma_z^2} \right]. \quad (A4)$$

APPENDIX B: NONLINEAR OPERATOR FOR MOMENTUM EQUATIONS AND ENERGY EQUATION

The non-linear operator $N(\epsilon(\mathbf{u}_{inc} + \mathbf{u}_{ref}))$ in the x direction can be expanded as

$$\begin{aligned} N_x(\epsilon(\mathbf{u}_{inc} + \mathbf{u}_{ref})) &= \epsilon^2 (u_{inc}^x + u_{ref}^x) \frac{\partial(u_{inc}^x + u_{ref}^x)}{\partial x} \\ &\quad + \epsilon^2 (u_{inc}^z + u_{ref}^z) \frac{\partial(u_{inc}^x + u_{ref}^x)}{\partial z}. \end{aligned} \quad (B1)$$

It is known that non-linear operator vanishes at the leading order; if it is separately applied to the incident internal wave beam or the reflecting internal wave beam, therefore only cross-terms remain at the leading order; therefore at the leading order $O(\epsilon^2)$, the non-linear operator in the x direction can be given as

$$\begin{aligned} N_x(\epsilon(\mathbf{u}_{inc} + \mathbf{u}_{ref})) &= \epsilon^2 u_{inc}^x \frac{\partial u_{ref}^x}{\partial x} + \epsilon^2 u_{inc}^z \frac{\partial u_{ref}^x}{\partial z} \\ &\quad + \epsilon^2 u_{ref}^x \frac{\partial u_{inc}^x}{\partial x} + \epsilon^2 u_{ref}^z \frac{\partial u_{inc}^x}{\partial z} \\ &= -2\epsilon^2 k_x A_{inc}^x A_{ref}^x (\cos \phi_{inc} \sin \phi_{ref} \\ &\quad + \cos \phi_{ref} \sin \phi_{inc}) \\ &= -2\epsilon^2 k_x A_{inc}^x A_{ref}^x \sin(\phi_{inc} + \phi_{ref}) \\ &= -2\epsilon^2 k_x A_{inc}^x A_{ref}^x \sin(2k_x x - 2\omega t + \phi_0). \end{aligned} \quad (B2)$$

Similarly, $N(\epsilon(\mathbf{u}_{inc} + \mathbf{u}_{ref}))$ in the z direction can be expanded as

$$\begin{aligned} N_z(\epsilon(\mathbf{u}_{inc} + \mathbf{u}_{ref})) &= \epsilon^2(u_{inc}^x + u_{ref}^x) \frac{\partial(u_{inc}^z + u_{ref}^z)}{\partial x} \\ &\quad + \epsilon^2(u_{inc}^z + u_{ref}^z) \frac{\partial(u_{inc}^z + u_{ref}^z)}{\partial z}. \end{aligned} \quad (\text{B3})$$

The same argument applies here, and only cross-terms remain at the leading order $O(\epsilon^2)$ and it can be given as

$$\begin{aligned} N_z(\epsilon(\mathbf{u}_{inc} + \mathbf{u}_{ref})) &= \epsilon^2 u_{inc}^x \frac{\partial u_{ref}^z}{\partial x} + \epsilon^2 u_{inc}^z \frac{\partial u_{ref}^z}{\partial z} \\ &\quad + \epsilon^2 u_{ref}^x \frac{\partial u_{inc}^z}{\partial x} + \epsilon^2 u_{ref}^z \frac{\partial u_{inc}^z}{\partial z} \\ &= -\frac{2\epsilon^2 k_x^2}{k_z} A_{inc}^x A_{ref}^x (\cos \phi_{inc} \sin \phi_{ref} \\ &\quad - \cos \phi_{ref} \sin \phi_{inc}) \\ &= \frac{2\epsilon^2 k_x^2}{k_z} A_{inc}^x A_{ref}^x \sin(\phi_{inc} - \phi_{ref}) \\ &= -\frac{2\epsilon^2 k_x^2}{k_z} A_{inc}^x A_{ref}^x \sin(2k_z z + \phi_0). \end{aligned} \quad (\text{B4})$$

These are the resultant terms from the non-linear operator in the momentum equations; however, a similar type of procedure is also followed for the non-linear operator in the energy equation $N_\rho(\epsilon(\rho_{inc} + \rho_{ref}), \epsilon(\mathbf{u}_{inc} + \mathbf{u}_{ref}))$ as follows:

$$\begin{aligned} N_\rho(\epsilon(\rho_{inc} + \rho_{ref}), \epsilon(\mathbf{u}_{inc} + \mathbf{u}_{ref})) &= \epsilon^2(u_{inc}^x + u_{ref}^x) \frac{\partial(\rho_{inc} + \rho_{ref})}{\partial x} \\ &\quad + \epsilon^2(u_{inc}^z + u_{ref}^z) \frac{\partial(\rho_{inc} + \rho_{ref})}{\partial z}. \end{aligned} \quad (\text{B5})$$

Also, the non-linear terms of the energy equation vanish at the leading order $O(\epsilon^2)$ if the non-linear operator is only applied to the incident internal wave beam or the reflecting internal wave beam. Therefore, again only cross-terms remain in the non-linear operator of the energy equation, and it can be given as

$$\begin{aligned} N_\rho(\epsilon(\rho_{inc} + \rho_{ref}), \epsilon(\mathbf{u}_{inc} + \mathbf{u}_{ref})) &= \epsilon^2 u_{inc}^x \frac{\partial \rho_{ref}}{\partial x} + \epsilon^2 u_{inc}^z \frac{\partial \rho_{ref}}{\partial z} \\ &\quad + \epsilon^2 u_{ref}^x \frac{\partial \rho_{inc}}{\partial x} + \epsilon^2 u_{ref}^z \frac{\partial \rho_{inc}}{\partial z} \\ &= \epsilon^2 k_x A_{inc}^x Q_{ref}^x (\cos \phi_{inc} \cos \phi_{ref} + \cos \phi_{ref} \cos \phi_{inc}) \\ &\quad + \epsilon^2 k_x A_{ref}^x Q_{inc}^x (\cos \phi_{inc} \cos \phi_{ref} + \cos \phi_{ref} \cos \phi_{inc}) \\ &= \epsilon^2 k_x (A_{inc}^x Q_{ref}^x + A_{ref}^x Q_{inc}^x) \cos(2k_z z + \phi_0). \end{aligned} \quad (\text{B6})$$

APPENDIX C: THE SECOND HARMONIC INTEGRATION

The amplitude of the second harmonic velocity in the x direction is given by the integral

$$A_{2\omega_0}^x = \gamma_{2\omega_0} \exp(-\alpha_{2\omega_0} \xi_{2\omega_0}) \int \exp(\alpha_{2\omega_0} \xi_{2\omega_0}) F_{2\omega_0} d\xi_{2\omega_0}, \quad (\text{C1})$$

where $\gamma_{2\omega_0} = -2(k_z^{2\omega_0} \omega)^2 / C g_{2\omega_0} N_0^2 k_x$ and $\alpha_{2\omega_0} = \nu N^2 k_x^2 / 2C g_{2\omega_0} \omega^2$ and the function inside the integral is given as

$$F_{2\omega_0} = A_{inc}^x A_{ref}^x \sin(k_z^{2\omega_0} z - \phi_0). \quad (\text{C2})$$

First, the function in Eq. (C2) is given in the $x-z$ coordinate as

$$\begin{aligned} F_{2\omega_0}(x, z) &= A_0 A_{ref} \exp(-\alpha((2x - x_{ref}) \cos \theta - z_{ref} \sin \theta)) \\ &\quad \times \exp\left(-\frac{\sin^2 \theta(2x^2 - 2x x_{ref} + x_{ref}^2)}{2\sigma^2}\right) \\ &\quad \times \exp\left(-\frac{\cos^2 \theta(2z^2 - 2z z_{ref} + z_{ref}^2)}{2\sigma^2}\right) \\ &\quad \times \exp\left(\frac{\sin 2\theta(x_{ref} z_{ref} - x z_{ref} - z x_{ref})}{2\sigma^2}\right) \\ &\quad \times \sin(k_z^{2\omega_0} z - \phi_0). \end{aligned} \quad (\text{C3})$$

Note that in Eq. (C3), the angle θ is the angle obtained in the coordinate transformation of the incident internal wave beam and also the reflection angle $\theta_r = -\theta$. Moreover, x_{ref} and z_{ref} are the coordinates of the intersection point where the incident internal wave beam's centreline reaches $z = H$. Having said these, Eq. (C3) can be given in a more compact form as follows:

$$F_{2\omega_0}(x, z) = D_{2\omega_0} \exp(\alpha_x x^2 + \beta_x x + \alpha_z z^2 + \beta_z z) \sin(k_z^{2\omega_0} z - \phi_0), \quad (\text{C4})$$

where

$$\begin{aligned} D_{2\omega_0} &= A_0 A_{ref} \exp(-\alpha(z_{ref} \sin \theta - x_{ref} \cos \theta)) \\ &\quad \times \exp\left(\frac{\sin 2\theta x_{ref} z_{ref} - x_{ref}^2 \sin^2 \theta - z_{ref}^2 \cos^2 \theta}{2\sigma^2}\right), \end{aligned} \quad (\text{C5})$$

$$\alpha_x = -\frac{2 \sin^2 \theta}{2\sigma^2}, \quad (\text{C6})$$

$$\beta_x = \frac{2x_{ref} \sin^2 \theta}{2\sigma^2} - 2\alpha \cos \theta - \frac{z_{ref} \sin 2\theta}{2\sigma^2}, \quad (\text{C7})$$

$$\alpha_z = -\frac{2 \cos^2 \theta}{2\sigma^2}, \quad (\text{C8})$$

$$\beta_z = \frac{2z_{ref} \cos^2 \theta}{2\sigma^2} - \frac{x_{ref} \sin 2\theta}{2\sigma^2}. \quad (\text{C9})$$

To perform the integration, the integral should be written in the transformed coordinate system derived for the second harmonic signal. Its angle of rotation is given as $\theta_{2\omega_0}$. Before proceeding to the coordinate change of the forcing term, let us write it explicitly,

$$\begin{bmatrix} x - x_{ref} \\ z - z_{ref} \end{bmatrix} = \begin{bmatrix} \cos \theta_{2\omega_0} & -\sin \theta_{2\omega_0} \\ \sin \theta_{2\omega_0} & \cos \theta_{2\omega_0} \end{bmatrix} \begin{bmatrix} \xi_{2\omega_0} \\ \eta_{2\omega_0} \end{bmatrix}. \quad (\text{C10})$$

Under this coordinate change, the forcing term given in Eq. (C11) can be written as

$$\begin{aligned} F_{2\omega_0} &= G_{2\omega_0} \exp(\alpha_\xi \xi_{2\omega_0}^2 + \beta_\xi \xi_{2\omega_0} + \alpha_\eta \eta_{2\omega_0}^2 \\ &\quad + \beta_\eta \eta_{2\omega_0} + \chi \xi_{2\omega_0} \eta_{2\omega_0}) \sin(k_z^{2\omega_0} \sin \theta_{2\omega_0} \xi_{2\omega_0} \\ &\quad + k_z^{2\omega_0} \cos \theta_{2\omega_0} \eta_{2\omega_0} + k_z^{2\omega_0} z_{ref} - \phi_0), \end{aligned} \quad (\text{C11})$$

where

$$G_{2\omega_0} = D_{2\omega_0} \exp(\alpha_x x_{ref}^2 + \beta_x x_{ref} + \alpha_z z_{ref}^2 + \beta_z z_{ref}), \quad (\text{C12})$$

$$\alpha_\xi = \alpha_x \cos^2 \theta_{2\omega_0} + \alpha_z \sin^2 \theta_{2\omega_0}, \quad (\text{C13})$$

$$\begin{aligned} \beta_\xi &= 2\alpha_x \cos \theta_{2\omega_0} x_{ref} + \beta_x \cos \theta_{2\omega_0} \\ &\quad + 2\alpha_z \sin \theta_{2\omega_0} z_{ref} + \beta_z \sin \theta_{2\omega_0}, \end{aligned} \quad (\text{C14})$$

$$\alpha_\eta = \alpha_x \sin^2 \theta_{2\omega_0} + \alpha_z \cos^2 \theta_{2\omega_0}, \quad (\text{C15})$$

$$\begin{aligned} \beta_\eta &= -2\alpha_x \sin \theta_{2\omega_0} x_{ref} - \beta_x \sin \theta_{2\omega_0} \\ &\quad + 2\alpha_z \cos \theta_{2\omega_0} z_{ref} + \beta_z \cos \theta_{2\omega_0}, \end{aligned} \quad (\text{C16})$$

$$\chi = 2(\alpha_z - \alpha_x) \sin \theta_{2\omega_0} \cos \theta_{2\omega_0}. \quad (\text{C17})$$

The integration given in Eq. (C1) is in the direction of $\xi_{2\omega_0}$; therefore, the terms which are independent of $\xi_{2\omega_0}$ can be directly taken out of the integral. In this way, sine terms can be expanded to take out the mentioned terms as

$$\begin{aligned} &\sin(k_z^{2\omega_0} \sin \theta_{2\omega_0} \xi_{2\omega_0} + \varphi(\eta_{2\omega_0})) \\ &= \sin(k_z^{2\omega_0} \sin \theta_{2\omega_0} \xi_{2\omega_0}) \cos(\varphi(\eta_{2\omega_0})) \\ &\quad + \cos(k_z^{2\omega_0} \sin \theta_{2\omega_0} \xi_{2\omega_0}) \sin(\varphi(\eta_{2\omega_0})), \end{aligned} \quad (\text{C18})$$

where $\varphi(\eta_{2\omega_0}) = k_z^{2\omega_0} \cos \theta_{2\omega_0} \eta_{2\omega_0} + k_z^{2\omega_0} z_{ref} - \phi_0$. As a result of this trigonometric identity, the integral can be performed in two parts: The first part can be given as

$$\begin{aligned} &\int \exp(\alpha_\xi \xi_{2\omega_0}^2 + (\beta_\xi + \alpha_{2\omega_0}) \xi_{2\omega_0} + \chi \xi_{2\omega_0} \eta_{2\omega_0}) \\ &\quad \times \sin(k_z^{2\omega_0} \sin \theta_{2\omega_0} \xi_{2\omega_0}) d\xi_{2\omega_0} = \text{Im} \left(\int \exp(\alpha_\xi \xi_{2\omega_0}^2 \right. \\ &\quad \left. + (\beta_\xi + \alpha_{2\omega_0} + ik_z^{2\omega_0} \sin \theta_{2\omega_0}) \xi_{2\omega_0} + \chi \xi_{2\omega_0} \eta_{2\omega_0}) d\xi_{2\omega_0} \right). \end{aligned} \quad (\text{C19})$$

The integral in Eq. (C19) can be taken by the method of stationary phase. This method requires to find the maxima of the function inside the exponential term. Therefore, the integral above can be formulated as

$$\begin{aligned} &\int \exp(\zeta(\xi_{2\omega_0})) d\xi_{2\omega_0} \\ &= \int \exp(\zeta(\xi_{2\omega_0}^0) + \frac{\zeta''(\xi_{2\omega_0}^0)}{2} (\xi_{2\omega_0} - \xi_{2\omega_0}^0)^2) d\xi_{2\omega_0} \\ &= \exp(\zeta(\xi_{2\omega_0}^0)) \int \exp\left(\frac{\zeta''(\xi_{2\omega_0}^0)}{2} (\xi_{2\omega_0} - \xi_{2\omega_0}^0)^2\right) d\xi_{2\omega_0}, \end{aligned} \quad (\text{C20})$$

where $\xi_{2\omega_0}^0$ is obtained by finding the root of $\zeta'(\xi_{2\omega_0}^0) = 0$ which can be explicitly given as

$$\xi_{2\omega_0}^0 = -\frac{\beta_\xi + \alpha_{2\omega_0} + ik_z^{2\omega_0} \sin \theta_{2\omega_0} + \chi \eta_{2\omega_0}}{2\alpha_\xi}. \quad (\text{C21})$$

Therefore, the result of the integral in Eq. (C19) can be approximately obtained as

$$\begin{aligned} &-\sqrt{-\frac{\pi}{\alpha_\xi}} \exp\left(-\frac{(\beta_\xi + \alpha_{2\omega_0} + \chi \eta_{2\omega_0})^2}{4\alpha_\xi}\right) \exp\left(\frac{(k_z^{2\omega_0} \sin \theta_{2\omega_0})^2}{4\alpha_\xi}\right) \\ &\quad \times \sin\left(\frac{k_z^{2\omega_0} \sin \theta_{2\omega_0} (\beta_\xi + \alpha_{2\omega_0} + \chi \eta_{2\omega_0})}{2\alpha_\xi}\right). \end{aligned} \quad (\text{C22})$$

Similarly, the second part of the integral can be given as

$$\begin{aligned} &\int \exp(\alpha_\xi \xi_{2\omega_0}^2 + (\beta_\xi + \alpha_{2\omega_0}) \xi_{2\omega_0} + \chi \xi_{2\omega_0} \eta_{2\omega_0}) \cos \\ &\quad \times (k_z^{2\omega_0} \sin \theta_{2\omega_0} \xi_{2\omega_0}) d\xi_{2\omega_0} = \text{Re} \left(\int \exp(\alpha_\xi \xi_{2\omega_0}^2 + (\beta_\xi \right. \\ &\quad \left. + \alpha_{2\omega_0} + ik_z^{2\omega_0} \sin \theta_{2\omega_0}) \xi_{2\omega_0} + \chi \xi_{2\omega_0} \eta_{2\omega_0}) d\xi_{2\omega_0} \right). \end{aligned} \quad (\text{C23})$$

The same procedure is followed and the result of the integral (C23) can be obtained as

$$\begin{aligned} &\sqrt{-\frac{\pi}{\alpha_\xi}} \exp\left(-\frac{(\beta_\xi + \alpha_{2\omega_0} + \chi \eta_{2\omega_0})^2}{4\alpha_\xi}\right) \exp\left(\frac{(k_z^{2\omega_0} \sin \theta_{2\omega_0})^2}{4\alpha_\xi}\right) \\ &\quad \times \cos\left(\frac{k_z^{2\omega_0} \sin \theta_{2\omega_0} (\beta_\xi + \alpha_{2\omega_0} + \chi \eta_{2\omega_0})}{2\alpha_\xi}\right). \end{aligned} \quad (\text{C24})$$

After combining all results, the solution to Eq. (C1) is obtained as

$$A_{2\omega_0}^x = H_{2\omega_0} \exp(-\alpha_{2\omega_0} \xi_{2\omega_0}) \exp(\hat{\phi}(\eta_{2\omega_0})) \sin(\hat{\phi}(\eta_{2\omega_0})), \quad (\text{C25})$$

where

$$H_{2\omega_0} = G_{2\omega_0} \gamma_{2\omega_0} \sqrt{-\frac{\pi}{\alpha_\xi}} \exp\left(\frac{(k_z^{2\omega_0} \sin \theta_{2\omega_0})^2}{4\alpha_\xi}\right), \quad (\text{C26})$$

$$\hat{\phi}(\eta_{2\omega_0}) = \varphi(\eta_{2\omega_0}) - \frac{k_z^{2\omega_0} \sin \theta_{2\omega_0} (\beta_\xi + \alpha_{2\omega_0} + \chi \eta_{2\omega_0})}{2\alpha_\xi}, \quad (\text{C27})$$

$$\hat{\phi}(\eta_{2\omega_0}) = \alpha_\eta \eta_{2\omega_0}^2 + \beta_\eta \eta_{2\omega_0} - \frac{(\beta_\xi + \alpha_{2\omega_0} + \chi \eta_{2\omega_0})^2}{4\alpha_\xi}. \quad (\text{C28})$$

APPENDIX D: INVISCID ANALYTICAL SOLUTION

Momentum equations under stream function formulation where $u = \psi_z$, $w = -\psi_x$, and the energy equation in our configuration where the slope $\alpha = 0^\circ$ are given as

$$\rho_t + \psi_x + J(\rho, \psi) = 0, \quad (\text{D1})$$

$$\nabla^2 \psi_t - \rho_x + J(\nabla^2 \psi, \psi) = 0, \quad (\text{D2})$$

where $J(a, b) = a_x b_z - a_z b_x$ is the Jacobian term. The analytical solution by TAL assumes that the solution is in the form of

$$\begin{aligned} \psi &= \epsilon \left\{ Q(x, z) e^{-i\omega t} + c.c \right\} + \epsilon^2 Q_0(x, z) \\ &\quad + \epsilon^2 \left\{ Q_2(x, z) e^{-2i\omega t} + c.c \right\}, \end{aligned} \quad (\text{D3})$$

$$\begin{aligned} \rho &= \epsilon \left\{ R(x, z) e^{-i\omega t} + c.c \right\} + \epsilon^2 R_0(x, z) \\ &\quad + \epsilon^2 \left\{ R_2(x, z) e^{-2i\omega t} + c.c \right\}, \end{aligned} \quad (\text{D4})$$

where

$$Q = Q^{inc} + Q^{ref}. \quad (\text{D5})$$

They satisfy no flux boundary condition at $z = 0$. After substituting the prescribed solutions (D3) and (D4) into Eqs. (D1) and (D2), the forced equation for second harmonic wave is obtained as

$$(4 \sin^2 \theta - 1)Q_{2xx} + (4 \sin^2 \theta)Q_{2zz} = f_2(x, z), \quad (\text{D6})$$

where

$$f_2(x, z) = -3i \sin \theta J(\nabla^2 Q, Q). \quad (\text{D7})$$

And also

$$R_2(x, z) = -\frac{iQ_{2x}}{2 \sin \theta} + h_2(x, z), \quad (\text{D8})$$

where

$$h_2(x, z) = -\frac{1}{2 \sin^2 \theta} \{J(Q_x, Q)\}. \quad (\text{D9})$$

In the particular profile analyzed here, it is easier to use the velocity field than the stream function, as the incident internal wave amplitude has a Gaussian profile multiplied with the complex exponential which is given as

$$\begin{aligned} A_x^{inc}(\eta) &= e^{-\frac{\eta^2}{2\sigma^2}} e^{ik_\eta^0 \eta} = \int_0^\infty \hat{A}_x^{inc}(k_\eta) e^{ik_\eta^0 \eta} dk_\eta \\ &= \int_0^\infty \sigma \sqrt{2\pi} \exp(-\sigma^2(k_x - k_x^0)^2/2) e^{ik_x^0(x-z \cot \theta)} dk_x, \end{aligned} \quad (\text{D10})$$

where k_η^0 is the wave number where the envelope is distributed around. In terms of x and z , the rotated coordinate can be expressed as $\eta = x \sin \theta - z \cos \theta$ and the wave number multiplied with the position vector can be expressed as $k_\eta^0 \eta = k_x^0(x - z \cot \theta)$; therefore, the incident wave can be given as

$$A_x^{inc}(x, z) = e^{-\frac{(x \sin \theta - z \cos \theta)^2}{2\sigma^2}} e^{ik_x^0(x-z \cot \theta)} \quad (\text{D11})$$

and also

$$A_z^{inc}(x, z) = \frac{k_x^0}{k_z^0} e^{-\frac{(x \sin \theta - z \cos \theta)^2}{2\sigma^2}} e^{ik_x^0(x-z \cot \theta)}. \quad (\text{D12})$$

Similarly, the reflecting internal wave beam can be given as

$$\begin{aligned} A_x^{ref}(\eta_r) &= e^{-\frac{\eta_r^2}{2\sigma^2}} e^{ik_{\eta_r}^0 \eta_r} = \int_0^\infty \hat{A}_x^{ref}(k_{\eta_r}) e^{ik_{\eta_r}^0 \eta_r} dk_{\eta_r} \\ &= \int_0^\infty \sigma \sqrt{2\pi} \exp(-\sigma^2(k_x - k_x^0)^2/2) e^{ik_x^0(x+z \cot \theta)} dk_x, \end{aligned} \quad (\text{D13})$$

where $k_{\eta_r}^0$ is the wave number where the envelope is distributed around. In terms of x and z , the rotated coordinate can be expressed as $\eta_r = x \sin \theta + z \cos \theta$ and also the wave number multiplied with the position vector can be expressed as $k_{\eta_r}^0 \eta_r = k_x^0(x + z \cot \theta)$; therefore, the incident wave can be given as

$$A_x^{ref}(x, z) = e^{-\frac{(x \sin \theta + z \cos \theta)^2}{2\sigma^2}} e^{ik_x^0(x+z \cot \theta)} \quad (\text{D14})$$

and also

$$A_z^{ref}(x, z) = -\frac{k_x^0}{k_z^0} e^{-\frac{(x \sin \theta + z \cos \theta)^2}{2\sigma^2}} e^{ik_x^0(x+z \cot \theta)}. \quad (\text{D15})$$

As a result, the primary frequency velocity field can be given as

$$\begin{aligned} u &= e^{-\frac{(x \sin \theta - z \cos \theta)^2}{2\sigma^2}} e^{ik_x^0(x-z \cot \theta)} \\ &\quad + e^{-\frac{(x \sin \theta + z \cos \theta)^2}{2\sigma^2}} e^{ik_x^0(x+z \cot \theta)}, \end{aligned} \quad (\text{D16})$$

and

$$\begin{aligned} w &= \frac{k_x^0}{k_z^0} e^{-\frac{(x \sin \theta - z \cos \theta)^2}{2\sigma^2}} e^{ik_x^0(x-z \cot \theta)} \\ &\quad - \frac{k_x^0}{k_z^0} e^{-\frac{(x \sin \theta + z \cos \theta)^2}{2\sigma^2}} e^{ik_x^0(x+z \cot \theta)}. \end{aligned} \quad (\text{D17})$$

Under this formulation, there is no need to explicitly calculate the stream function for the primary mode. Furthermore, the second harmonic forcing term can be given as

$$J(\nabla^2 Q, Q) = u \frac{\partial}{\partial x} \left(\frac{\partial u}{\partial z} - \frac{\partial w}{\partial x} \right) + w \frac{\partial}{\partial z} \left(\frac{\partial u}{\partial z} - \frac{\partial w}{\partial x} \right). \quad (\text{D18})$$

Alternatively,

$$\begin{aligned} J(\nabla^2 Q, Q) &= -(u_{inc} + u_{ref}) \frac{\partial}{\partial x} (\omega_{inc} + \omega_{ref}) \\ &\quad - (w_{inc} + w_{ref}) \frac{\partial}{\partial z} (\omega_{inc} + \omega_{ref}), \end{aligned} \quad (\text{D19})$$

where $\omega_{inc} = \partial_x w_{inc} - \partial_z u_{inc}$ and $\omega_{ref} = \partial_x w_{ref} - \partial_z u_{ref}$ are vorticity fields induced by the incident and the reflecting internal wave beams,

$$\omega_{inc} = -2ik_x^0 e^{-\frac{(x \sin \theta - z \cos \theta)^2}{2\sigma^2}} e^{ik_x^0(x-z \cot \theta)} \quad (\text{D20})$$

and

$$\omega_{ref} = -2ik_x^0 e^{-\frac{(x \sin \theta + z \cos \theta)^2}{2\sigma^2}} e^{ik_x^0(x+z \cot \theta)}. \quad (\text{D21})$$

Moreover, it is known that the incident and the reflecting internal wave beams are exact non-linear solutions on their own; they vanish in Eq. (D2), and therefore, only terms appearing due to interaction between the incident and the reflecting wave beam result in non-zero forcing of the second harmonic in Eq. (D2) which can be given as

$$\begin{aligned} J(\nabla^2 Q, Q) &= -u_{inc} \frac{\partial \omega_{ref}}{\partial x} - w_{inc} \frac{\partial \omega_{ref}}{\partial z} \\ &\quad - u_{ref} \frac{\partial \omega_{inc}}{\partial x} - w_{ref} \frac{\partial \omega_{ref}}{\partial z}. \end{aligned} \quad (\text{D22})$$

Therefore,

$$f_2(x, z) = -24i \sin \theta (k_x^0)^2 e^{-\frac{(x \sin \theta)^2}{\sigma^2}} e^{-\frac{(z \cos \theta)^2}{\sigma^2}} e^{2ik_x^0 x}. \quad (\text{D23})$$

The solution to Eq. (7) is found as

$$\begin{aligned} \hat{Q}_2(k_x; z) &= A_2(k_x) \exp \{ik_x z \cot \gamma_2\} \\ &\quad + B_2(k_x) \exp \{-ik_x z \cot \gamma_2\} + \frac{i \exp \{ik_x z \cot \gamma_2\}}{k_x \sin 2\gamma_2} \\ &\quad \times \int_{-\infty}^0 dz' \hat{f}_2(k_x, z') \exp \{-ik_x z' \cot \gamma_2\} \\ &\quad - \frac{i \exp \{-ik_x z \cot \gamma_2\}}{k_x \sin 2\gamma_2} \\ &\quad \times \int_{-\infty}^0 dz' \hat{f}_2(k_x, z') \exp \{ik_x z' \cot \gamma_2\}, \end{aligned} \quad (\text{D24})$$

where $\gamma_2 = \sin^{-1}(2 \sin \theta)$. In the case analyzed in this paper, the main focus is paid on the downward propagating wave; therefore, the boundary condition is chosen accordingly. As a result, only the first term satisfies the radiation condition; thus $B_2(k_x) = 0$. No flux boundary condition at $z = 0$ leads to

the following spectral amplitude of the downward propagating internal wave beam:

$$A_2(k_x) = -\frac{2}{k_x \sin 2\gamma_2} \int_{-\infty}^0 dz' \hat{f}_2(k_x, z') \sin \{k_x z' \cot \gamma_2\}. \quad (\text{D25})$$

Previously, it was also found that the mean flow is generated by the internal wave beam collision in inviscid setting.¹⁷ In that analysis, the stream function for mean flow is given as

$$-\mathcal{Q}_{0x} = J(\rho, Q) = w_0. \quad (\text{D26})$$

Equation (D26) can be explicitly given as

$$-\mathcal{Q}_{0x} = u_{\text{ref}} \frac{\partial \rho_{\text{inc}}}{\partial x} + u_{\text{inc}} \frac{\partial \rho_{\text{ref}}}{\partial x} + w_{\text{ref}} \frac{\partial \rho_{\text{inc}}}{\partial z} + w_{\text{inc}} \frac{\partial \rho_{\text{ref}}}{\partial z}, \quad (\text{D27})$$

where $u = u_{\text{inc}} + u_{\text{ref}}$, $w = w_{\text{inc}} + w_{\text{ref}}$, and $\rho = \rho_{\text{inc}} + \rho_{\text{ref}}$. It should also be noted that $\rho_{\text{inc}} = iw_{\text{inc}}/\sin \theta$ and $\rho_{\text{ref}} = iw_{\text{ref}}/\sin \theta$. If these are plugged into Eq. (D27), the mean velocity in the z direction can be expressed as

$$-\mathcal{Q}_{0x} = \frac{2(k_x^0)^2}{k_z^0 \sin \theta} e^{-\frac{(x \sin \theta)^2}{\sigma^2}} e^{-\frac{(z \cos \theta)^2}{\sigma^2}} \cos(2 \cot \theta k_x^0 z) = w_0. \quad (\text{D28})$$

¹Akylas, T. R., Grimshaw, R. H. J., Clarke, S. R., and Tabaei, A., "Reflecting tidal wave beams and local generation of solitary waves in the ocean thermocline," *J. Fluid Mech.* **593**, 297–313 (2007).

²Allshouse, M. R., Lee, F. M., Morrison, P. J., and Swinney, H. L., "Internal wave pressure, velocity, and energy flux from density perturbations," *Phys. Rev. Fluids* **1**, 014301 (2016).

³Azevedo, A., da Silva, J. C. B., and New, A. L., "On the generation and propagation of internal solitary waves in the southern Bay of Biscay," *Deep Sea Res., Part I* **53**, 927–941 (2006).

⁴Bordes, G., Venaille, A., Joubaud, S., Odier, P., and Dauxois, T., "Experimental observation of a strong mean flow induced by internal gravity waves," *Phys. Fluids* **24**, 086602 (2012).

⁵Diamessis, P. J., Wunsch, S., Delwiche, I., and Richter, P., "Nonlinear generation of harmonics through the interaction of an internal wave beam with a model oceanic pycnocline," *Dyn. Atmos. Oceans* **66**, 110–137 (2014).

- ⁶Dossmann, Y., Auclair, F., and Paci, A., "Topographically induced internal solitary waves in a pycnocline: Secondary generation and selection criteria," *Phys. Fluids* **25**, 066601 (2013).
- ⁷Garrett, C. and Kunze, E., "Internal tide generation in the deep ocean," *Annu. Rev. Fluid Mech.* **39**, 57–87 (2007).
- ⁸Ghaemsaidi, S. J., "Interference and resonance of internal gravity waves," Ph.D. thesis, Massachusetts Institute of Technology, MIT, Cambridge, Massachusetts, 2015.
- ⁹Grisouard, N. and Staquet, C., "Numerical simulations of the local generation of internal solitary waves in the Bay of Biscay," *Nonlinear Processes Geophys.* **17**, 575–584 (2010).
- ¹⁰Grisouard, N., Staquet, C., and Gerkema, T., "Internal and interfacial tides: Beam scattering and local generation of solitary waves," *J. Mar. Res.* **59**, 227–255 (2001).
- ¹¹Grisouard, N., Staquet, C., and Gerkema, T., "Generation of internal solitary waves in a pycnocline by an internal wave beam: A numerical study," *J. Fluid Mech.* **676**, 491–513 (2011).
- ¹²Lighthill, J., *Waves in Fluids* (Cambridge University Press, 1978).
- ¹³Mathur, M. and Peacock, T., "Internal wave beam propagation in nonuniform stratifications," *J. Fluid Mech.* **638**, 133–152 (2009).
- ¹⁴Rodenborn, B., Kifer, D., Zhang, H. P., and Swinney, H. L., "Harmonic generation by reflecting internal waves," *Phys. Fluids* **23**, 026601 (2011).
- ¹⁵Sutherland, B., *Internal Gravity Waves* (Cambridge University Press, 2010).
- ¹⁶Tabaei, A. and Akylas, T. R., "Nonlinear internal gravity wave beams," *J. Fluid Mech.* **482**, 141–161 (2003).
- ¹⁷Tabaei, A., Akylas, T. R., and Lamb, K. G., "Nonlinear effects in reflecting and colliding internal wave beams," *J. Fluid Mech.* **526**, 217–243 (2005).
- ¹⁸Thorpe, S. A., *The Turbulent Ocean* (Cambridge University Press, 2005).
- ¹⁹van den Bremer, T. S. and Sutherland, B. R., "The mean flow and long waves induced by two-dimensional internal gravity wavepackets," *Phys. Fluids* **26**, 106601 (2014).
- ²⁰Wunsch, S. and Brandt, A., "Laboratory experiments on internal waves interactions with a pycnocline," *Exp. Fluids* **53**, 1663–1679 (2012).
- ²¹Wunsch, S., Ku, H., Delwiche, I., and Awadallah, R., "Simulations of nonlinear harmonic generation by an internal wave beam incident on a pycnocline," *Nonlinear Processes Geophys.* **21**, 855–868 (2014).
- ²²Wunsch, S., Delwiche, I., Frederick, G., and Brandt, A., "Experimental study of nonlinear harmonic generation by internal waves incident on a pycnocline," *Exp. Fluids* **56**(5), 87 (2015).
- ²³Zhou, Q. and Diamessis, P. J., "Reflection of an internal gravity wave beam off a horizontal free slip surface," *Phys. Fluids* **25**, 036601 (2013).